Journal of Drug Delivery Science and Technology 86 (2023) 104691

Contents lists available at ScienceDirect

Journal of Drug Delivery Science and Technology

journal homepage: www.elsevier.com/locate/jddst

In vitro and *in vivo* evaluation of multi-target-directed Rivastigmine/Memantine/*Gingko biloba*-loaded nanofibers against Alzheimer's disease

Servan Veysanoglu [a,1], Busra Ertas [a,b,1], Ece Guler [a,c,j], Fadime Topal [a], Gul Sinemcan Ozcan [d], Gokhan Duruksu [d], Burak Ece [e], Cansun Sahin Cam [f], Oguzhan Aydemir [g,h], Muhammet Emin Cam [a,b,c,i,j,k,l,*]

[a] Department of Pharmacology, Faculty of Pharmacy, Marmara University, İstanbul, 34854, Turkiye
[b] Genetic and Metabolic Diseases Research and Investigation Center, Marmara University, İstanbul, 34722, Turkiye
[c] Center for Nanotechnology and Biomaterials Application and Research, Marmara University, İstanbul, 34722, Turkiye
[d] Stem Cell and Gene Therapies Research and Applied Center, Medical Faculty, Kocaeli University, Kocaeli, 41380, Turkiye
[e] Department of Electrical and Electronics Engineering, Faculty of Technology, Marmara University, İstanbul, 34722, Turkiye
[f] Department of Psychiatry, Faculty of Medicine, Marmara University, İstanbul, 34854, Turkiye
[g] Department of Pharmacology, Faculty of Pharmacy, İstinye University, İstanbul, 34010, Turkiye
[h] Department of Research & Development, Joker Food Industry International Domestic and Foreign Trade Company, İstanbul, 34885, Turkiye
[i] Biomedical Engineering Department, University of Aveiro, 3810-193, Aveiro, Portugal
[j] MecNano Technologies, Cube Incibation, Teknopark İstanbul, İstanbul, 34906, Turkiye
[k] SFA R&D Laboratories, Teknopark İstanbul, İstanbul, 34906, Turkiye
[l] ATA BIO Technology, Teknopol İstanbul, İstanbul, 34930, Turkiye

ARTICLE INFO

Keywords:
Alzheimer's disease
Rivastigmine
Memantine
Gingko biloba
Sublingual administration

ABSTRACT

The highly complex pathophysiology of Alzheimer's disease (AD) and the low bioavailability of the currently used drugs make it necessary to offer versatile treatment options. In this study, polyvinyl alcohol (PVA)/polyvinylpyrrolidone (PVP) nanofibers (NFs) were loaded with rivastigmine (RIV), memantine (MM), and *Gingko biloba* (GB) extract, and their anti-Alzheimer's effects were investigated *in vitro* by cell culture and *in vivo* by animal experiments. The characterization studies, including FTIR, XRD, and DSC analysis, showed that the fibers exhibited a good compatibility. The rapid disintegration (in 5.2 s) and complete dissolution (in 120 s) of RIV/MM/GB-loaded NF indicated their suitability for sublingual application. Cell viability analysis revealed that RIV/MM/GB-loaded NFs can be considered as safe and promising candidates. RIV/MM/GB-loaded NFs tremendously improved the learning and memory impairment seen in the AD model created by the injection of intracerebroventricular-streptozotocin into rats. Moreover, RIV/MM/GB-loaded NF stimulated stem cells to improve neuronal differentiation properties and significantly decreased the level of β-amyloid, tau, APP, TNF-α, AChE, and GSK-3β in the brain. The histopathological and immunostaining assays demonstrated that RIV/MM/GB-loaded NF reduced β-amyloid formation and tau hyperphosphorylation in the hippocampus and cerebral cortex. Thus, a novel and promising treatment strategy could be developed that has several advantages, such as ease of sublingual administration, reduced frequency of administration associated with lower drug amounts, and finally reduced toxicity and cost.

1. Introduction

Alzheimer's disease (AD) is an extremely complex disease that begins with amyloid-β accumulation and neuronal loss, resulting in neurobiochemical changes in the hippocampus and cerebral cortex, such as intracellular neurofibrillary tangles and extracellular senile plaque formation leading to progressive behavioural, emotional, and cognitive disorders [1]. According to the current data, 60% of 50 million dementia patients are AD, and this number is estimated to increase 4 times by 2050 [2]. In terms of its economic-financial burden, the current cost of

* Corresponding author. Department of Pharmacology, Faculty of Pharmacy, Marmara University, İstanbul, 34854, Turkiye.
E-mail address: muhammet.cam@marmara.edu.tr (M.E. Cam).
[1] Contributed equally to this work.

https://doi.org/10.1016/j.jddst.2023.104691
Received 25 February 2023; Received in revised form 11 June 2023; Accepted 16 June 2023
Available online 26 June 2023

the disease is about 1 trillion US dollars per year, and it is estimated to double by 2030 [3]. The increasing prevalence of AD brings with it a decrease in the well-being of the patient and society [4].

FDA-approved N-Methyl-*d*-aspartate receptor (NMDAR) antagonist (memantine) and acetylcholinesterase (AChE) inhibitors (rivastigmine, donepezil, galantamine) are currently used in symptomatic therapy [5]. Rivastigmine (RIV) is an acetylcholinesterase and butyrylcholinesterase inhibitor, which is thought to facilitate slowing down the cleavage of acetylcholine secreted by functionally intact cholinergic neurons. Memantine (MM) is a voltage-dependent, moderate affinity, and non-competitive NMDAR antagonist. MM prevents the effects of pathologically elevated glutamate levels that may lead to neuronal dysfunction [6]. Current treatments for AD do not show sufficient effectiveness in the progressive course of the disease. Therefore, studies focusing on the potential therapeutic efficacy of many herbs and their major compounds on AD are meticulously followed. Many plants such as *Ginkgo biloba* (GB), *Curcuma longa*, and *Salvia officinalis* are widely utilized by animal studies and AD patients [7]. Standardized GB extract is prescribed due to mechanisms of GB action including powerful antioxidant effects and potential inhibition of β-amyloid aggregation [8]. GB also increases blood flow and oxygen use in the brain. GB, which improves brain function and strengthens memory, slows down the progression of AD in the early stages [9]. It also inhibits the age-related decline of muscarinic acetylcholine receptors and alpha-2 adrenoceptors with improved acetylcholine uptake in the hippocampus [10].

The treatment of AD should be able to offer many solutions at the same time [11]. The literature has offered that the success rate of treatments with single agents is lower than that of treatments with combinations of agents in the AD treatment [12–15]. In the advanced stages of AD, patient compliance is low due to difficulty swallowing and forgetting to take the drugs [16]. Patient compliance with the therapeutic regimen affects the effectiveness of the treatment [17]. Therefore, decreasing the frequency of dosage is crucial for patient compliance, especially in AD. There is a disadvantage of the currently used treatments in that the pharmaceutical dosage forms of these drugs are suitable for oral use, hence, the bioavailability of the drug exposed to the first-pass effect decreases in the body [18]. According to the studies, it offers a potential approach to drugs to be developed for the treatment of neurological diseases due to the advantages of the sublingual application [19]. The sublingual regions are highly vascularized, and the drugs are fastly absorbed through the sublingual blood vessels. Therefore, drugs administered by the sublingual route do not undergo hepatic first-pass metabolism and their bioavailability increases. This route of administration may be preferred for drugs that degrade in the gastrointestinal tract and/or undergo high hepatic clearance and/or for patients that have dysphagia [20]. Among potential drug delivery systems, nanofibers (NFs) have many features such as mechanical strength, extensive surface area, flexibility, porous structure, and low-cost [21]. Furthermore, although suitably delivering many drugs at the same time is usually a challenging topic, this problem can be eliminated with NFs [22].

We designed a novel sublingual drug delivery system that can offer a versatile solution for AD treatment with some advantages such as easy to take, less frequency of dosage (three drugs at once), a lower amount of drug, and hence, lower toxicity and lower cost. Anti-Alzheimer's activity of RIV/MM/GB-loaded NFs was evaluated by *in vitro* and *in vivo* studies. In addition, its neuroprotective effect was evaluated by behavioural tests in an animal model of AD.

2. Experimental

2.1. Chemicals

RIV (Mw ~ 250.337 g/mol), MM (Mw ~ 179.3 g/mol), PVA (Mw ~ 89,000–98,000 g/mol), (PVP, Mw ~ 40,000 g/mol), and all solvents were taken from Sigma Aldrich. All purchased materials are best suited for analytical assays due to their being high-purity reagents.

2.2. Preparation of Ginkgo biloba plant extracts

Ginkgo biloba leaves were collected from Istanbul Province and extracted with 3 mL of concentrated hydrochloric acid and 5 mL of water for 2.5 h. The Soxhlet extraction was performed in a Soxhlet apparatus at 60 °C for 6 h. Shaker extraction was performed at 200 rpm at 25 °C. The resulting liquid extract was then filtered through Whatman filter paper. Extraction was performed with the same solid-to-solvent ratio of 5 g of ground leaf sample and 50 mL of EtOH (99.7%, v/v) (see Figure S2) [23].

2.3. Preparation, optimization, and characterization of solutions

PVP and PVA were each dissolved at 15% w/v in deionized water. PVA/PVP was mixed in ratios 8:2, 5:5, and 2:8 (v/v) by continuous magnetic stirring, respectively. The fibers produced from the solution formed at the determined ratios of polymers were examined by SEM. MM (12.6 mg/mL), RIV (0.63 mg/mL), and GB (12.6 mg/mL) were loaded in the 8:2 ratio PVA/PVP polymer blend that has a beadless and homogeneous fiber appearance compared to the other two ratios. The concentrations of drugs for solutions were determined according to the dosage of drugs that will be given to rats (RIV- 1 mg/kg [24]; MM- 20 mg/kg [25]; and GB-20 mg/kg [26]).

The physical parameters of polymer solutions were measured using a force tensiometer (Kruss K9, Hamburg, Germany), viscometer (DV-E, Brookfield AMETEK, USA), density bottle (10 mL pycnometer bottle, Boru Cam Inc., Turkey), and conductivity probe (Cond 3110 SET 1, WTW, Germany). All measurements were carried out at room temperature and constant humidity.

2.4. Manufacturing of electrospun fiber

Electro-spinning used in fiber production has many parameters that affect fiber morphology. These parameters are polymer/solvent ratio, flow rate, spinneret-collector distance, needle diameter, and applied voltage [27]. The high-voltage power supplier (0–30 kV) was attached to the syringe. The spinneret-collector distance was 15 cm and its flow rate was kept between 0.1 and 0.5 mL/h. The metallic needle (21 G) was used. The PVA/PVP polymer blends at three different ratios were used to produce the fiber with the best morphology. According to SEM images, the polymer blend used for the production of fibers with the desired morphology was selected and the drugs were added to this polymer blend.

2.5. Scanning electron microscope (SEM)

The diameters and morphological analyzes of the fibers were characterized by SEM (EVO LS 10, ZEISS SEM instrument). The fiber samples which were analyzed using SEM were coated with gold using a sputter coater (SC 7620 model, Quorum Technologies, ABD) for 60 s, and observed by SEM with an accelerating voltage of 5 kV. The average fiber diameter was measured using Image J software from randomly selected SEM images.

2.6. Fourier transform infrared spectroscopy (FTIR)

The chemical structures of all the compounds used in the production of fibers and the interactions between these compounds were examined by FTIR (Jasco FTIR 4700 spectrometer). The wavelength value of the FTIR device ranges between 400 and 4000 cm^{-1} [28].

2.7. Differential scanning calorimeter (DSC)

The thermal property of the fibers was analyzed by DSC (PerkinElmer Jade DSC) and Pyris software (PerkinElmer Inc., Mass., USA) under a dynamic argon atmosphere (20 mL min^{-1}) at a temperature range of 0–350 °C at a heating rate of 10 °C min^{-1}.

2.8. X-ray powder diffraction (XRD)

XRD spectra of the crystalline phases of the powders and composite nanofiber were recorded by a D/Max-BR diffractometer (RigaKu, Tokyo, Japan) using Cu Kα radiation. Analysis was performed at 40 mV and 30 mA over the 2θ range of 0–80° at a rate of 2° min^{-1}. The software program of the XRD device was used for obtaining the results.

2.9. Mechanical properties of the fibers

Before the tensile test, the thickness of the fibers was measured using a digital micrometer (Mitutoyo MTI Corp., USA). The tensile strength of the fibers was measured and evaluated using a tensile test machine (Shimadzu, EZ-LX, China) at ambient conditions. The obtained data were analyzed using Bluehill 2 software (Elancourt, France). Six fiber samples (1 × 5 cm) were tested for each sample set. Both ends of each specimen were clamped horizontally between the upper and lower handles with a distance between grips of 1 cm. A tensile test was performed under conditions of a test speed of 5 mm min^{-1}.

2.10. Drug encapsulation efficiency

Encapsulation efficiency is a parameter that gives the percentage of drugs successfully loaded into NFs. In this study, RIV/MM/GB-loaded NFs were first weighed at 5 mg, and then, it was completely dissolved in 10 mL of deionized water in a volumetric flask. The flask was gently mixed overnight to completely dissolve RIV, MM, and GB from the fibers into the solvent. 1 mL of solution was taken and then RIV, MM, and GB were detected by a UV–visible spectrophotometer at 271, 274, and 247 nm, respectively. All measurements were repeated in a triplicate [29].

$$\textit{Encapsulation efficiency} : \textit{mass of actual drug loaded in nanofibers} \,/\, \textit{mass of used in nanofiber fabrication} \; x\; 100\% \quad (1)$$

2.11. Disintegration and wetting test

A circular section of 3 cm diameter was cut off from the fibers and placed into 15 mL of simulated saliva. The preparation of simulated saliva has been clearly described in our previous study [30]. The disintegration and wetting of the fibers were recorded using a video camera (Canon Sx70 HS, Tokyo, Japan) at 50 frames/sec.

2.12. Dissolution test

The dissolution test was done to investigate the release kinetics of RIV/MM/GB-loaded NFs. Thus, RIV, MM, and GB were prepared in 5 different concentrations (2, 4, 6, 8, and 10 μg/mL for RIV and GB; 2.8, 5.6, 8.4, 11.2, 14 mg/mL for MM) to construct linear calibration curves for each. 15 mL of simulated saliva at 37 °C was mixed in a 7 cm diameter Petri dish at 150 rpm on a multi-point stirrer. After these procedures for simulating sublingual administration, NFs loaded with RIV/MM/GB were cut into 5 mg each as a circle and dropped into the simulated saliva [31]. 1 mL of the supernatant was removed at pre-determined time points (2.5, 5, 7.5, 10, 15, 30, 45, 60, 90, and 120 s) and replaced with 1 mL of pre-warmed simulated saliva (prepared as described in the previous section) to maintain a constant volume. RIV, MM, and GB dissolution profiles were examined by UV spectroscopy at 271 [32], 274 [33], and 247 [34] nm, respectively. Experiments were carried out in triplicate.

2.13. In vitro drug release kinetic test

Five different mathematical models benefited to analyze and interpret drug release kinetics from nanofibers. The drug release kinetics were investigated with Korsmeyer-Peppas (2), zero-order (3), first-order (4), Higuchi (5), and Hixson-Crowell models (6). N is the marker of the drug release mechanism as a diffusion exponent. The fractional amount of drug release at time t was represented by Q. K, K_0, K_1, K_h, and K_{hc}, which are kinetic constants, belong to Korsmeyer-Peppas, zero order, first order, Higuchi, and Hixson-Crowell models, respectively.

$$Q = Kt^n \quad (2)$$

$$Q = K_0 t \quad (3)$$

$$\ln(1-Q) = -K_1 t \quad (4)$$

$$Q = K_h t^{1/2} \quad (5)$$

$$Q^{1/3} = K_{hc} t \quad (6)$$

2.14. Cell viability assay (WST)

For the cell culture studies, NFs were prepared in uniform circular shapes of 6.0 ± 0.5 mm in diameter by punching out a piece of NF sheet. Each piece was placed into the well of a 48-well culture plate and cultured with a 500 μL medium. Human foreskin fibroblasts (P3; 10,000 cells/cm^2) were seeded on NFs and cultured for 48 h in a humidified CO_2 incubator at 37 °C. After 48 h, the medium was replaced with DMEM (Gibco, Thermo, Paisley, UK) with 10% WST-1 (Roche). Fibroblasts were incubated for an additional 1 h. Cell viability was measured at 450 nm in a spectrophotometer (Molecular Devices). The results were compared with the number of cells cultured without NF in the medium (control). Cytotoxicity was expressed as a percentage of cell viability compared to the control [35].

2.15. Cell culture and differentiation

The effect of the RIV/MM/GB release was evaluated concerning cytotoxicity on fibroblast cells and the stem cell plasticity on human dental pulp stem cells (DP-SCs) *in vitro*. Stem cells used in this study were previously isolated and characterized [36]. DP-SCs were cultured in DMEM supplemented with 10% FBS (Gibco) and 1% penicillin-streptomycin (Gibco) at 37 °C in a humidified atmosphere containing 5% CO_2. After cells reached 70–80% confluency, cells were detached by 0.25% trypsin-EDTA (Gibco), washed with phosphate-buffered saline (PBS; Gibco), and re-plated at the ratio of 1:4 for subculture. The culture medium was refreshed once every 2–3 days.

For neurogenic differentiation, cells at passage 3 were cultivated until 70–80% confluency. The culture medium was replaced with a differentiation medium, which consists of DMEM supplemented with 0.5 mM isobutylmethylxanthine (IBMX, Sigma–Aldrich, St.Louis, MO), 10 ng/mL brain-derived neurotrophic factor (BDNF), epidermal growth factor (EGF, Biological Industries, Kibbutz Beit Haemek, Israel), basic Fibroblast growth factor (bFGF, Sigma–Aldrich), neural stem cell proliferation supplements (Stem Cell Technologies Inc., Vancouver, British Columbia, Canada), and 1% penicillin-streptomycin. Then, cells were cultured for 7 days in a differentiation medium refreshing every 2–3 days with the defined differentiation medium.

2.16. Gene expression analysis

The alteration in the gene expression profile of some neuronal differentiation markers in DP-SCs was evaluated after the cell differentiation [37]. The results were compared to the gene expression of cell culture in the culture medium without NFs (control). Total RNA was extracted by Aurum Total RNA Mini Kit (Bio-Rad, Hercules, CA) according to the protocol supplied by the manufacturer. The RNA concentration (A260) and quality (A260/A280 ratio) were determined using a PicoDrop spectrophotometer (Picodrop Limited, Hinxton, UK). The total RNA was used to synthesize the cDNA by iScript cDNA Synthesis Kit (Biorad) according to the protocol supplied by the manufacturer. The gene expression level of BDNF, glial fibrillary acidic protein (GFAP), Tubb3, Nestin, neuronal differentiation 1 (NeuroD1), and neurogenin 2 (Neurog2) were evaluated by using iTaq Universal SYBR Green Supermix (Biorad). Using the LightCycler 480-II system (Roche), the PCR amplification followed a two-step cycling program: 30-sec pre-denaturation at 95 °C, 45 cycles at 95 °C for 15 s, and 60 °C for 60 s. Cp values were determined by LightCycler 480 Software (release 1.5), and a melt curve analysis was conducted to evaluate the specificity of the reaction. ActB gene amplification was used as a housekeeping gene in the calculations. The sequence of the primers was given in Table 1.

2.17. Animals

Forty-eight male/female Wistar albino rats (250–350 g) were obtained from Marmara University The Experimental Animal Implementation and Research Center (DEHAMER). Rats were kept in cages with suitable conditions (controlled temperature (22 ± 2 °C), humidity (40–60%), and light (12 h/12 h light/dark regime)) throughout the experiment. The animals were kept in each of the polyacrylic cages for no more than 4 animals and animals were provided with unlimited access to feed and water. The study was approved by the Local Institutional Animal Ethical Committee of Marmara University (with code 79.2019. mar). The Ethics Committee Guidelines were followed while working with the animals.

2.17.1. Intracerebroventricular administration of streptozotocin

Ketamine (100 mg/kg) and xylazine (10 mg/kg) were used for anesthetization. After the animals were fixed to the stereotaxis device, the bregma point was determined in the skull that was opened. By adopting the bregma reference point, the injection site was determined as anteroposterior, −0.8 mm from the bregma; lateral, ±1.5 mm from the sagittal suture; and ventral, −3.1 mm from the skull. STZ (3 mg/kg; 5 μl/each site) was injected bilateral icv into the holes opened from the determined points. While the animals in the treatment and model groups received STZ, animals in the sham group received the same volume of saline (0.9%, 5 μl at each site) instead of STZ. For wound care, the incision site was cleaned daily with the help of an antiseptic. Post-operative care of the animals was done meticulously to avoid any contamination due to head surgery. Two animals were placed in each cage and feed and water were left in the cage to allow them to heal for 3 days.

Table 1
Primer list of neuronal markers for gene expression analysis.

Gene Name	Forward Sequence (5′-3′)	Reverse Sequence (5′-3′)
Brain derived neurotrophic factor (BDNF)	gagctgagcgtgtgtgacag	gcaaaaagagaattggctggcg
Glial fibrillary acidic protein (GFAP)	tcctcaggggagatgatggt	ttctcgatgtagctggcaaag
Tubulin, beta 3 (TUBB3)	catggacagtgtccgctcag	caggcagtcgcagttttcac
Nestin	ctctgacctgtcagaagaat	gacgctgacacttacagaat
Neuronal differentiation 1 (NeuroD1)	gttatgagactatcactgctcaggacc	agaagttgccattgatgctgagc
Neurogenin 2 (Neurog2)	atccgagcagcactaacacg	gctgaggcacagttagagcc
Actin, beta (Actb)	tggcaccacaccttctacaatgagc	gcacagcttctccttaatgtcacgc

2.17.2. Experimental design of animal study

Icv injection of STZ is widely preferred in preclinical studies in terms of reflecting AD holistically, from cognitive deficit to neurochemical changes in the brain. As is well-known, the icv administration of STZ triggers amyloid deposition by disrupting the balances in the insulin signaling pathway and energy metabolism [38–40]. The second issue is that in drug research for AD, it is necessary to continue working for an appropriate period to determine the drug effects of the treatment period and to conduct behavioural tests. The last days of the study period were determined as behavioural tests [41,42].

In this study, the neurotherapeutic effect of RIV/MM/GB-loaded NF in the AD model has been investigated. Waiting for 3 days after the operation, it was ensured that the anxiety caused by the surgery was eliminated in animals and the animals were purified from the effects of the operation [43]. The animals were divided randomly into 4 groups with 12 in each group as follows.

- Sham group: Sham-operated rats that were exposed to surgery and saline (0.9%) were injected bilaterally (5 μl/site). They received pure PVA/PVP NF therapy sublingually for 21 days.
- AD group: Icv-STZ-induced rats that were exposed to STZ (3 mg/kg) injected via icv. They received pure PVA/PVP NF therapy sublingually for 21 days.
- RIV/MM/GB-loaded NF group: RIV/MM/GB-loaded NF (RIV- 1 mg/kg; MM- 20 mg/kg; and GB-20 mg/kg) treatment rats that received RIV/MM/GB-loaded NF via sublingually for 21 days after icv-STZ injection.
- RIV/MM/GB powder group: RIV/MM/GB powder (RIV- 1 mg/kg; MM- 20 mg/kg; and GB-20 mg/kg) treatment rats that received raw RIV, MM, and GB drugs via oral route for 21 days after icv-STZ injection.

Behaviour studies started on the 11th day and the tests were carried out in the morning hours. On the day the behavioural tests were completed, the rats were sacrificed by cardiac puncture. The brain was quickly removed and then placed in a cool saline bath. The brains were divided in two from the middle. The left hemisphere was used for histopathological analysis (kept in 4% paraformaldehyde) and the hippocampus of the other half was stored at −80 °C for molecular examination. Tissues belonging to each group (n = 12) were studied with samples in the following distribution according to the analysis: (1) 6 for biochemical analysis, (2) 3 for histopathological analysis, and (3) 3 for immunohistochemical analysis.

2.18. Biochemical analysis

After removing the rat brain, hippocampus tissue was rapidly removed and excised. Tissues were homogenized in cold PBS solution by a homogenizer (IKA brand Ultra-Turrax T25, USA) to obtain a 10% (w/v) homogenate solution. After centrifuging the homogenate samples at 3000 g for 10 min, the supernatant was carefully separated and biochemical analysis was performed immediately. Following the preparation of tissue samples, amyloid-β, APP, tau, GSK-3β, AChE activity, TNF-α, and BDNF levels were determined using a commercial ELISA kit according to the procedure with the manufacturer's instructions.

2.19. Histological analysis

Brain tissues collected from different groups were fixed with 10% formalin for 24 h and decalcification was achieved. Serial dilute ethanol was used to dehydrate. After cleaning with toluene, the samples were

embedded in paraffin in a hot air oven. Paraffin blocks were cut with a thickness of 5 μm and taken on a glass slide. After staining with hematoxylin and eosin (H&E) dye, the sections of the brain regions were visualized with the help of a light microscope (LEICA DM 1000). The severity of the damaged neurons in the cerebral cortex (CA2) and hippocampus regions was scored semiquantitatively using a graded scale (0–3: score 0 = no damage, score 1 = mild damage, score 2 = moderate damage, and score 3 = severe damage). Degeneration of neurons was assessed as intensely stained nuclei, cytoplasmic vacuolation, swelling or shrinkage of the cell, and increase in perineuronal space. The average of the damage scores was calculated for each group and statistical analysis was performed.

2.20. Immunohistochemistry

For Amyloid-β and tau protein immunohistochemistry in brain tissues, samples of brain regions were taken on a positively charged slide in the form of sections with a thickness of four microns. Preparations were made for the dyeing process as previously described. Sections were incubated with primary antibodies ((anti-p-amyloid (ABCAM, ab10148) and anti-Tau (ABCAM, ab131354)) or PBS (negative control) at 4 °C overnight. Following this procedure, they were incubated with a biotinylated secondary antibody and incubated with HRP-conjugated streptavidin (ABCAM, ab236466) for 15 min. They were counterstained with hematoxylin and the analysis and scoring of antibody

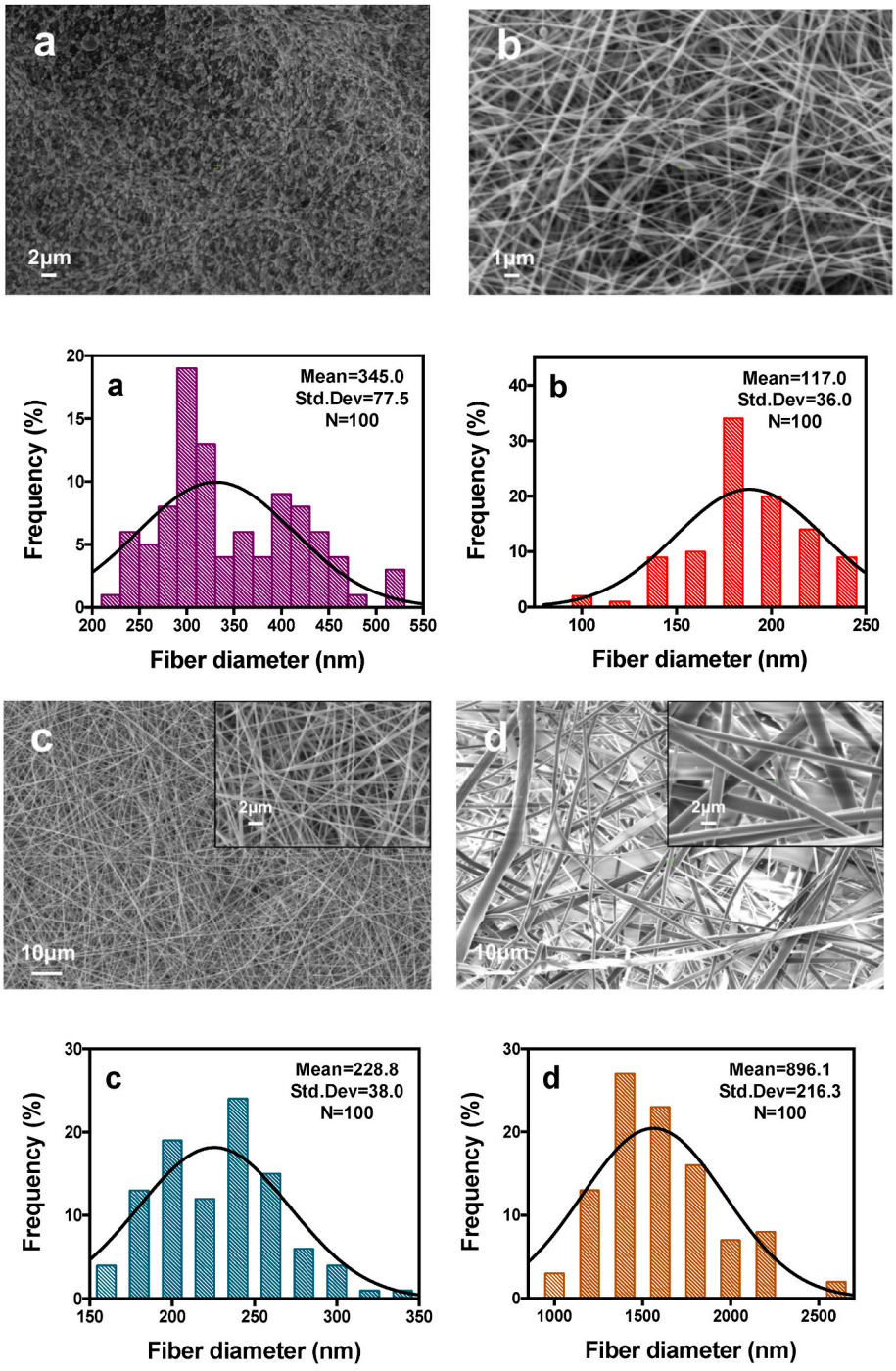

Fig. 1. Effects of PVA and PVP blend ratio on fiber morphology and diameter distribution graphs of pure PVA/PVP fiber at three different ratios: (a) 8:2, (b) 5:5, and (c) 8:2 (v/v); and drugs-loaded PVA/PVP fiber (8:2, v/v) (d).

expressions were performed with the aid of light microscopy.

2.21. Statistical analysis

All the results were analyzed using GraphPad Prism 8.0 statistical program. Data were expressed as mean ± SEM. Escape latency and path length analysis of the MWM test were performed with a two-way analysis of variance (ANOVA) analysis followed by the Bonferroni post hoc test. Other behavioural tests and biochemical analyzes were evaluated with one-way ANOVA analysis followed by Tukey's post hoc test. Data were analyzed for statistical significance by one-way or (ANOVA) and Tukey post hoc test. $p < 0.05$ was considered statistically significant.

3. Results

3.1. Optimization process and solution characterization

There are multiple production techniques in fiber production, but the most common method for producing nanoscale fiber is ES. Various parameters such as polymer concentration, feed rate, tip-collector distance, and applied voltage affect the morphology of NFs produced by the ES. In this study, PVA and PVP were dissolved in water and PVA/PVP mixture was prepared in three different ratios of 8:2, 5:5, and 2:8, respectively, and fibers were produced in these ratios.

Electrospun fibers were produced at 25 kV. An electrically grounded collector, which is a piece of aluminum foil, was placed at a vertical distance of 15 cm. The syringe pump was fixed at 0.1 mL/h. The polymer solution was thrown into the grounded collector and the fiber was produced. SEM images were examined and the drugs were loaded in PVA/PVP composite with the 8:2 ratio, which has the best morphology. RIV (0.63 mg/mL), MM (12.6 mg/mL), and GB (12.6 mg/mL) were mixed with the polymer solution.

The same electrospinning parameters used in pure PVA/PVP fibers were also used in the production of drugs-loaded PVA/PVP fibers. Physical parameters for pure and drug-loaded fibers were examined. Density and viscosity increased from 1.025 g/mL and 4179 mPas to 1.032 g/mL and 4921 mPas, respectively; electrical conductivity and surface tension decreased from 648 μS/cm and 155.42 mN/m to 326 μS/cm and 127 mN/m, respectively with the adding of drugs (See Figure S3).

3.2. Morphological characterization of nanofibers

Fig. 1 shows the morphologies and diameters of pure and drug-loaded fibers analyzed by SEM. The PVA (15%, w/v) and PVP (15%, w/v) solutions were prepared at the rate of 2:8, 5:5, and 8:2 for pure fiber production. To produce the beadless, smooth, and homogeneous fiber surface, the flow rate was applied between 0.1 and 0.8 mL/h. The working distance was chosen between 12 and 18 cm and the voltage was applied between 18 and 30 kV. Pure fiber with desired properties was produced under the following conditions: PVA/PVP (8:2) polymer mixture, a flow rate of 0.1 mL/h, the applied electric current at 25 kV, and a working distance of 15 cm. The PVA/PVP (5:5) polymer mixture was produced at a flow rate of 0.4 mL/h, the applied voltage at 26 kV, and a working distance of 15 cm. The PVA/PVP (2:8) polymer mixture was produced at a flow rate of 0.3 mL/h, the applied voltage at 19 kV, and a working distance of 15 cm. The SEM images of the produced fibers were examined and the polymer solution with a PVA/PVP ratio of 8:2 was chosen as the optimized ratio due to its beadless, smooth, and homogeneous fiber surface, and MM, RIV, and GB were added to the PVA/PVP polymer solution at this ratio. The proportion of polymer solutions that the PVA/PVP fiber diameters 345.0 ± 77.5 nm, 117.0 ± 36.0 nm, and 228.8 ± 38.0 nm are 2:8, 5:5, and 8:2 respectively. The diameter of the loaded PVA/PVP (8:2) fiber is 896.1 ± 216.3 nm. It is seen that the diameter of the drug-loaded fibers increased in the SEM results. Beads in the fiber decreased when the PVA ratio increased.

3.3. Fourier transform infrared spectroscopy (FTIR)

The FTIR spectra of pure MM, RIV, GB, PVA, PVP, pure PVA/PVP NF, and RIV/MM/GB-loaded NF were demonstrated in Supporting Information, Figure S4. The peaks at 3501.60 cm^{-1}, 2732.64 cm^{-1}, and 1720.19 cm^{-1} are absorption peaks of RIV [44]. These peaks are H-bonded O–H, C–H, and C═O stretching vibrations, respectively. For RIV, the characteristic absorption peak is the C–N stretching of the amine group at 1278.57 cm^{-1}. C–H stretching bands between 2975.62 and 2836.77 cm^{-1} are characteristic absorption peaks of the MM [45]. The FTIR spectrum of GB shows the presence of O–H stretching at 3440 cm^{-1} and C–H stretching vibration at 2920 cm^{-1}. The carboxyl C═O, aromatic C═C, and C–O stretching peaks of GB were detected at 1740 cm^{-1}, 1620 cm^{-1}, and 1390 cm^{-1}, respectively [46]. The peaks for the H- bonded –OH stretching at 3272.07 cm^{-1}, $–CH_3$ stretching at 2908.97 cm^{-1}, C═O stretching at 1711.09 cm^{-1}, and C–O stretching bands at 1023.53 cm^{-1} belong to PVA [47]. The H-bonded O–H stretching at 3440.46 cm^{-1}, $–CH_3$ stretching at 2941.28 cm^{-1}, C═O stretching at 1649.32 cm^{-1}, and C–O stretching bands at 1016.30 cm^{-1} are assigned to PVP [48]. RIV/MM/GB-loaded NF was analyzed in FTIR spectroscopy. A strong absorption peak at 1650.77 cm^{-1} and a large peak at 3311.18 cm^{-1} were detected due to the carbonyl groups on PVP and the stretching of hydroxyl groups on PVA. The stretching vibrations of carbonyl of the ketone group at 1731.76 cm^{-1} and the C–H stretching band at 2915.84 cm^{-1} in the spectrum of RIV/MM/GB-loaded NF were associated with the structure of MM. The absorption peak of RIV belonging to the C–N stretching of the amine group was seen at 1288.22 cm^{-1} in RIV/MM/GB-loaded NF. It has been observed that drugs have been successfully loaded in PVA/PVP composite fiber.

3.4. Investigation of the thermal behaviour

DSC was analyzed range from 0 to 350 °C and the results were given in Supporting Information, Fig. S5. Glass transition temperature (Tg) and melting temperature (Tm) of pure and RIV/MM/GB-loaded PVP/PVA NF samples were analyzed. While Tg of PVP in the DSC curve of PVA/PVP NF is at 61.65 °C, the DSC curve for RIV/MM/GB-loaded NF displayed an endothermic transition at 66.74 °C was attributed to Tg of PVP [49]. The small endothermic peak in the drugs-loaded fibers positioned at about 204.76 °C was attributed to the Tm of PVA. The sharpness belonging to the Tm peak of PVA lessened due to the addition of drugs that have an amorphous structure and this peak shifted from 227.60 °C to 204.76 °C with the addition of drugs in polymer composite.

Ginkgo biloba showed four endothermal peaks due to the mixture of compounds [50]. Memantine exhibited Tm at 341 °C. Rivastigmine showed a sharp endothermic peak at 126 °C. Nevertheless, the reason why Tm and Tg values of drugs were not seen in the DSC curve of drug-loaded fibers is that drugs can be loaded homogeneously and successfully into the fibers [51]. Additionally, it was observed that the temperature difference between the transition from the glassy structure to the amorphous structure decreased after the drugs are added to the polymer composite. The reason for this difference can be a chemical interaction between drugs and the delivery system. Consequently, drug-loaded NFs are safe for application to the human body in the treatment of AD because the fibers are not melting at the human body temperature.

3.5. X-ray powder diffraction (XRD)

X-ray diffraction scans were used to analyze the structural and crystal forms of pure PVA, PVP, GB, MM, RIV, pure PVA/PVP NF, and RIV/MM/GB-loaded NF. The major peaks of MM, RIV, and GB were observed due to their crystal structure at $2\theta = 17.36°$, 18.74°, and 13.12°, respectively (Fig. S6 a-c) [52–54]. PVP is an amorphous polymer and possessed high Tg due to the existence of the rigid pyrrolidone group. Diffraction peaks belonging to PVP were detected at 19.98°

(Fig. S6d) [55]. In Fig. S6e, it has been observed at 2θ = 20.78° and 37.82° in the XRD pattern of pure PVA [56]. XRD patterns of pure PVA and PVP were also seen in pure PVA/PVP composite fiber at 2θ = 19.98°, 20.78°, and 37.82° (Fig. S6f). According to XRD results, the specific peaks belonging to PVA and PVP polymers were detected in pure and drug-loaded fibers samples (Fig. S6f). Compared to pure fiber, the peaks at 2θ = 17.36°, 18.76°, and 21.88° were observed in RIV/MM/GB-loaded PVA/PVP NF due to the drugs and it proves that drugs have been successfully loaded in NFs (Fig. S6g).

3.6. Tensile properties of nanofibers

The profile of tensile strength and strain at break of pure PVA/PVP and drugs-loaded NF were given in Supporting Information, Fig. S7. The tensile strength of pure fiber was 0.6386 MPa. The tensile strength of the drug-loaded fibers increased to 0.6935 MPa. The strain at the break of pure fibers was 32.23% and the strain at the break of drugs-loaded fiber was 57.12%. The drugs-loaded NFs were found more flexible than pure PVA/PVP NFs. According to these results, loading the drugs in NFs increased their mechanical strength and flexibility (Fig. S7c).

3.7. Disintegration and wetting test

RIV/MM/GB-loaded NFs were cut off circularly and then fibers were put in the middle of artificial saliva for wetting and disintegration tests. Fibers with hydrophilic properties got wet in 0.4 s and it was completely disintegrated in 5.2 s (Fig. 2).

3.8. In vitro dissolution test

An *in vitro* dissolution test was performed to examine the release kinetics of drugs in pharmaceutical formulations with rapid-release properties. The ability of RIV/MM/GB-loaded NF, which was designed for the sublingual application, to be dissolved in artificial saliva for 120 s was examined. According to Fig. 3, the dissolution rates of RIV, MM, and GB in the supernatant taken from the Petri dish in 60 s were 72.66, 76.84, and 50%, respectively. Drugs loaded into the fibers were observed to dissolve completely in 120 s.

3.9. In vitro release kinetic test

Table 2 displays the regression coefficients (R^2) and kinetic constants. Details of the kinetic model of RIV, MM, and GB release from fibers in phosphate buffer saline (pH 7.4) at 37 °C under dynamic conditions were shown in Fig. 4. Release kinetic models were preferred as Korsmeyer-Peppas, zero-order, first-order, Higuchi, and Hixon-Crowell. In the Korsmeyer-Peppas model, the n value represents the mechanism of drug release from the drug delivery system. This value is calculated according to the Korsmeyer formula and it determines the appropriate mechanism in drug release or evaluates the drug release resulting from drug delivery conforming to Fick's law or Fickian transport. It is also used to describe independent processes in drug delivery. The value of n, which better fits the release profile of drugs in a delivery system, determines the type of behaviour observed: Fickian models (case I) and non-Fickian models (case II, anomalous cases, and super case II).

In the Fickian model (case I), at n = 0.45, drug release is dominated by diffusion. Its kinetic is characterized by diffusivity. When n = 0.89, the model is non-Fickian (Case II), and the drug release rate corresponds to zero-order release kinetics. When 0.45 < n < 0.89, the model is non-Fickian or anomalous transport. The Super Case II model is characterized when n > 0.89.

3.10. Cell viability assay

In the cytotoxicity study using human fibroblast cells (P3), cell viability was measured with WST-1. It was calculated that drugs-loaded and pure NFs did not have any toxic effects on cells compared to control group cells, which were cultured in the medium without NFs. When the viability effects on cells were compared, there was no significant difference between the control and RIV/MM/GB-loaded NF groups (Fig. 5a). It was observed that the pure NF group promotes cell proliferation in comparison to RIV/MM/GB-loaded NF group ($p < 0.001$).

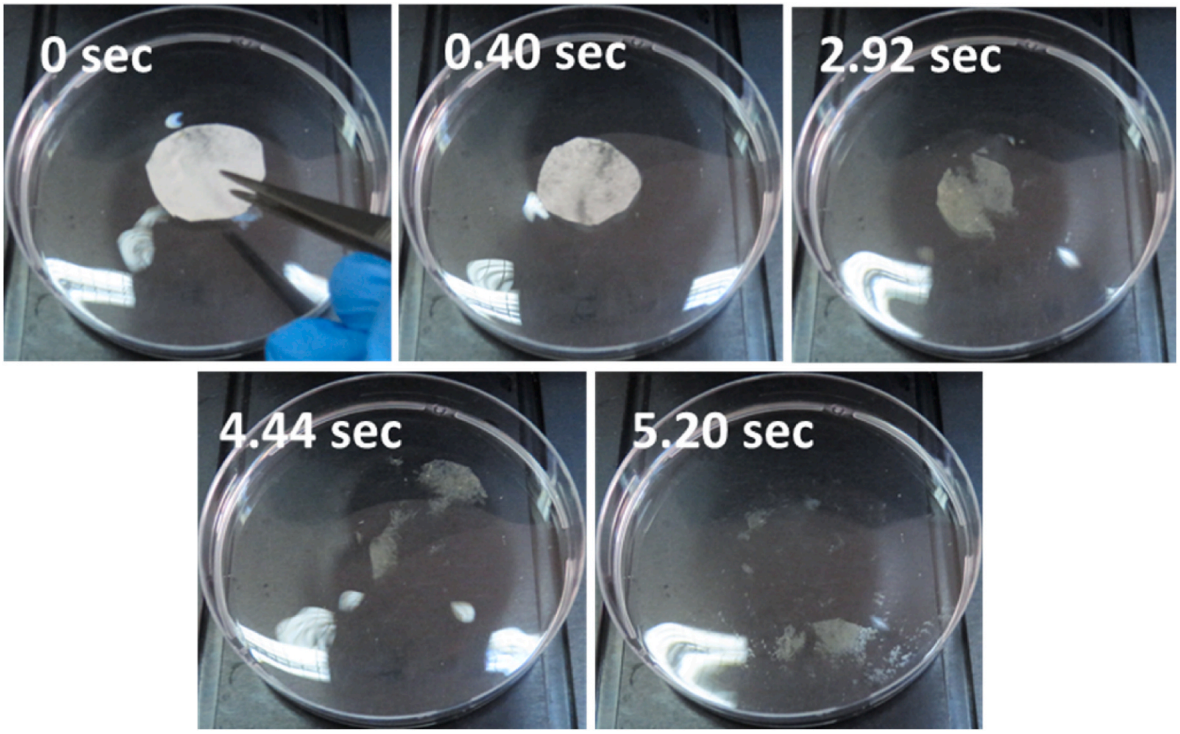

Fig. 2. Disintegration behaviour of RIV/MM/GB-loaded nanofibers at multiple time points during the disintegration test.

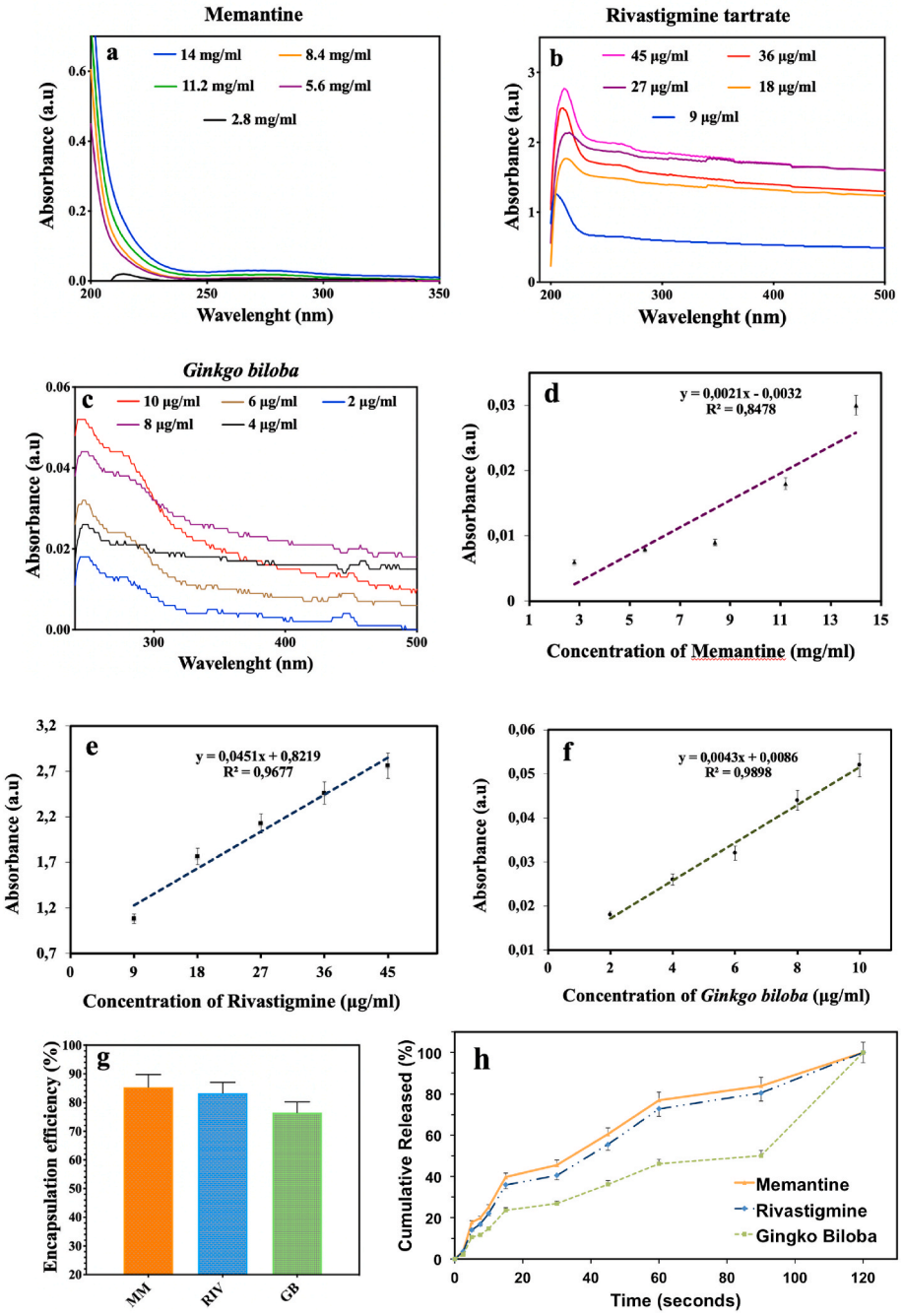

Fig. 3. *In vitro* dissolution profiles of nanofibers: Absorption spectra of different concentrations of memantine (a), rivastigmine tartrate (b), and *Ginkgo biloba* (c). Calibration curve of memantine (d), rivastigmine tartrate (e), *Ginkgo biloba* (f). Encapsulation efficiency (g) and dissolution profile (h) of RIV/MM/GB-loaded NF. All values were obtained using the average of three experiments with less than 5% error.

Table 2
Mathematical modeling of *in vitro* drug release kinetics for RIV/MM/GB-loaded NFs.

	Korsmeyer-Peppas		Zero Order		First Order		Higuchi		Hixson-Crowell	
Sample	R^2	n	R^2	K_0	R^2	K_1	R^2	K_h	R^2	K_{hc}
RIV	0,8978	0,8792	0,9084	0,7989	0,8821	−0,0137	0,9831	9,5742	0,9212	0,0324
MM	0,8999	0,8769	0,9092	0,8009	0,8851	−0,0137	0,9836	9,5967	0,9235	0,0325
GB	0,9356	0,8684	0,9309	0,6943	0,6628	−0,0117	0,8788	7,7720	0,7215	0,0280

3.11. Gene expression analysis

Exposure to RIV/MM/GB-loaded NFs produced a slight reduction in the cell viability of DP-SCs, but not a major difference. As seen in Fig. 5b, the control group DP-SCs did not differentiate into neuronal cells, while the same was true for pure NFs. On the other hand, the viability of pure NFs is higher compared to drug-loaded NFs. In addition, enhanced BDNF, Nestin, GFAP, and NeuroD1 expression of drug-loaded NFs was

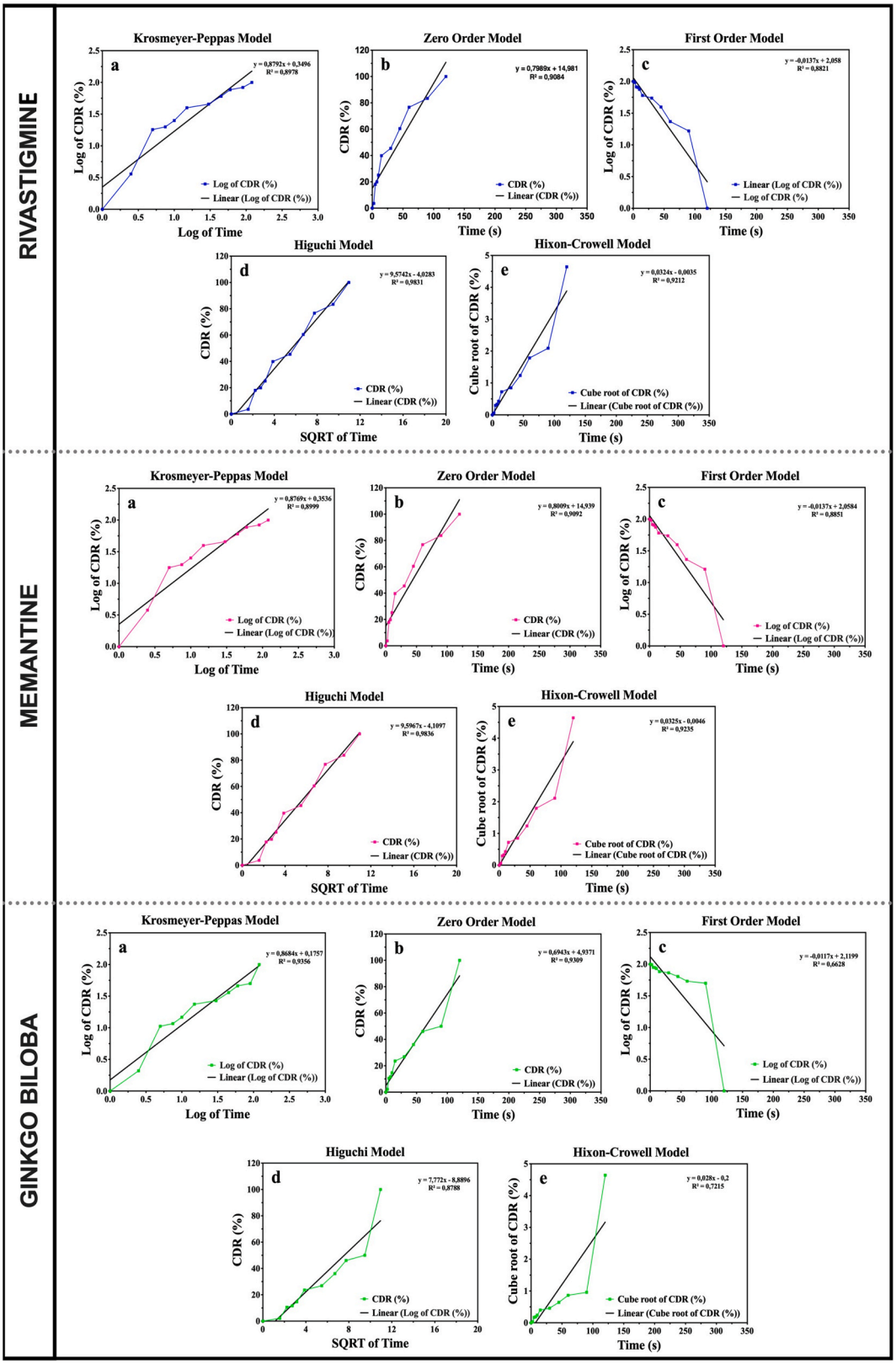

Fig. 4. Mathematical models of release profiles of Rivastigmine, Memantine, and *Gingko biloba* from RIV/MM/GB-loaded NFs in PBS (pH: 7.4).

4.38, 10.78, 4.38, and 3.18 fold, respectively, higher than for pure NFs. This differentiation occurred without the need for any chemical induction. The chemical cocktail significantly enhanced the neuronal differentiation of DP-SCs. Pure NFs slightly improved the expression of neuronal markers, but the Nestin and NeuroD1 expressions were estimated to be 18.38 and 6.23-fold higher compared to the undifferentiated control cells, respectively (Fig. 5c).

The effect of chemical induction on the cells with pure NF in the differentiation medium was significant concerning the expressions of NeuroD1 and neural progenitor cell marker, Nestin. The expression of Nestin

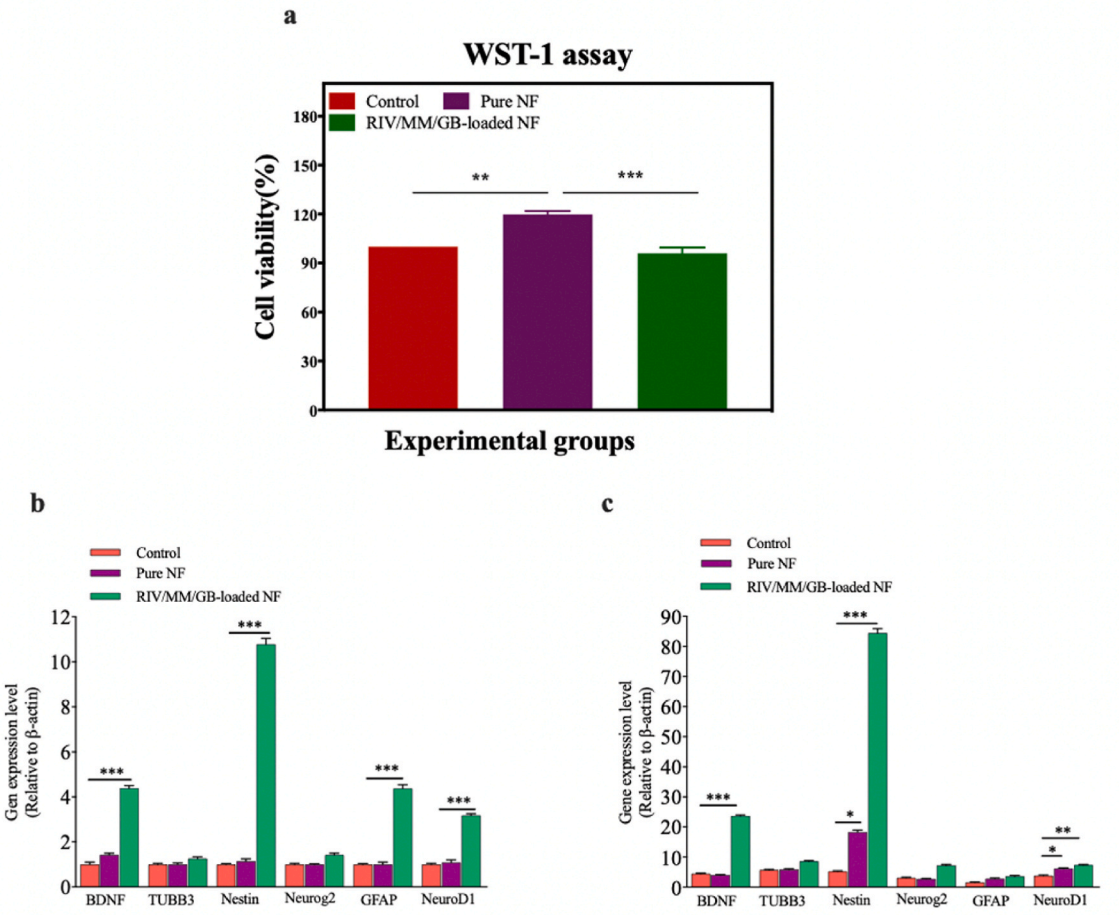

Fig. 5. (a) WST-1 assay of cell cytotoxicity. Gene expression levels (mRNA levels) of neuronal cell markers in DP-SCs compared with β-actin expression of undifferentiated control cells. While the level of brain-derived neurotrophic factor (BDNF), glial fibrillary acidic protein (GFAP), TUBB3, Nestin, neuronal differentiation 1 (NeuroD1), and neurogenin 2 (Neurog2) were analyzed after 7 days of culture in the culture medium (b), these values were evaluated in the neurogenic differentiation medium (c) at the same time. Significance differences were found at *$p < 0.05$, **$p < 0.01$ and ***$p < 0.001$.

and NeuroD1 in these cells was estimated 3.5 and 1.6-fold higher compared to the differentiated control cells, respectively. The expressions of BDNF and Nestin genes were calculated to be 23.59 and 84.45-fold higher with drugs-loaded NFs compared to the undifferentiated control cells and 5.32 and 15.89-fold higher compared to the differentiated control cells, respectively. The effect of drugs-loaded NFs was limited on the expressions of Neurog2 and GFAP and they showed 2.33 and 2.29-fold higher expression compared to the differentiated control cells.

3.12. Neurobehavioural observations

3.12.1. Locomotor activities

OFT was used for examining locomotion and exploratory behaviors of rats (Fig. 6). There were no significant differences between groups in latency to enter the center and time spent in the center zone(Fig. 6a–b). Moreover, no differences in the number of square crosses were seen between the groups (Fig. 6c) It was also recorded the number of groomings and feedings and found no significant differences between the groups (Fig. 6d–e). These data proved that the applied surgical procedure did not harm the motor functions of animals.

3.12.2. Short-term memory

In the acquisition phase, there was a significant ($p < 0.01$) difference in the exploration time between the sham group animals' familiar object and the new object, whereas in the other groups there was no such difference (Fig. 6f). The discrimination index analysis displayed that when compared to sham rats, AD rats were incapable of significantly ($p < 0.001$) differentiating between the familiar and novel object. In contrarily, treatment of these AD rats with RIV/MM/GB-loaded NF showed that they were capable of distinguishing between familiar and novel objects ($p < 0.01$) when compared to the AD rats (Fig. 6g). In addition, the RIV/MM/GB powder group also showed a significant ($p < 0.05$) rise compared to the AD group in the discrimination index. On the other hand, the preferential index analysis exhibited that AD rats were unable to significantly ($p < 0.001$) recognize the novel object when compared to the sham rats. Whereas, treatment of RIV/MM/GB-loaded NF showed that they were able to recognize the novel object when compared to the AD rats ($p < 0.01$) (Fig. 6h).

3.12.3. Passive avoidance

Mean initial latencies in the acquisition trial were not significantly different between all groups. The following day, the mean retention latency in the AD group was significantly ($p < 0.01$) decreased compared to the sham group (Fig. 6i). The decrease in retention latency in AD rats was significantly ($p < 0.05$) attenuated by RIV/MM/GB-loaded NF treatment, indicating improved memory retention. There was no significant change in the retention latency of the RIV/MM/GB powder group compared to the RIV/MM/GB loaded NF group.

3.12.4. Memory deficit and impairment of spatial learning ability

MWM was applied to assess working memory and spatial memory retention in rats. For spatial memory, the time to reach the platform was

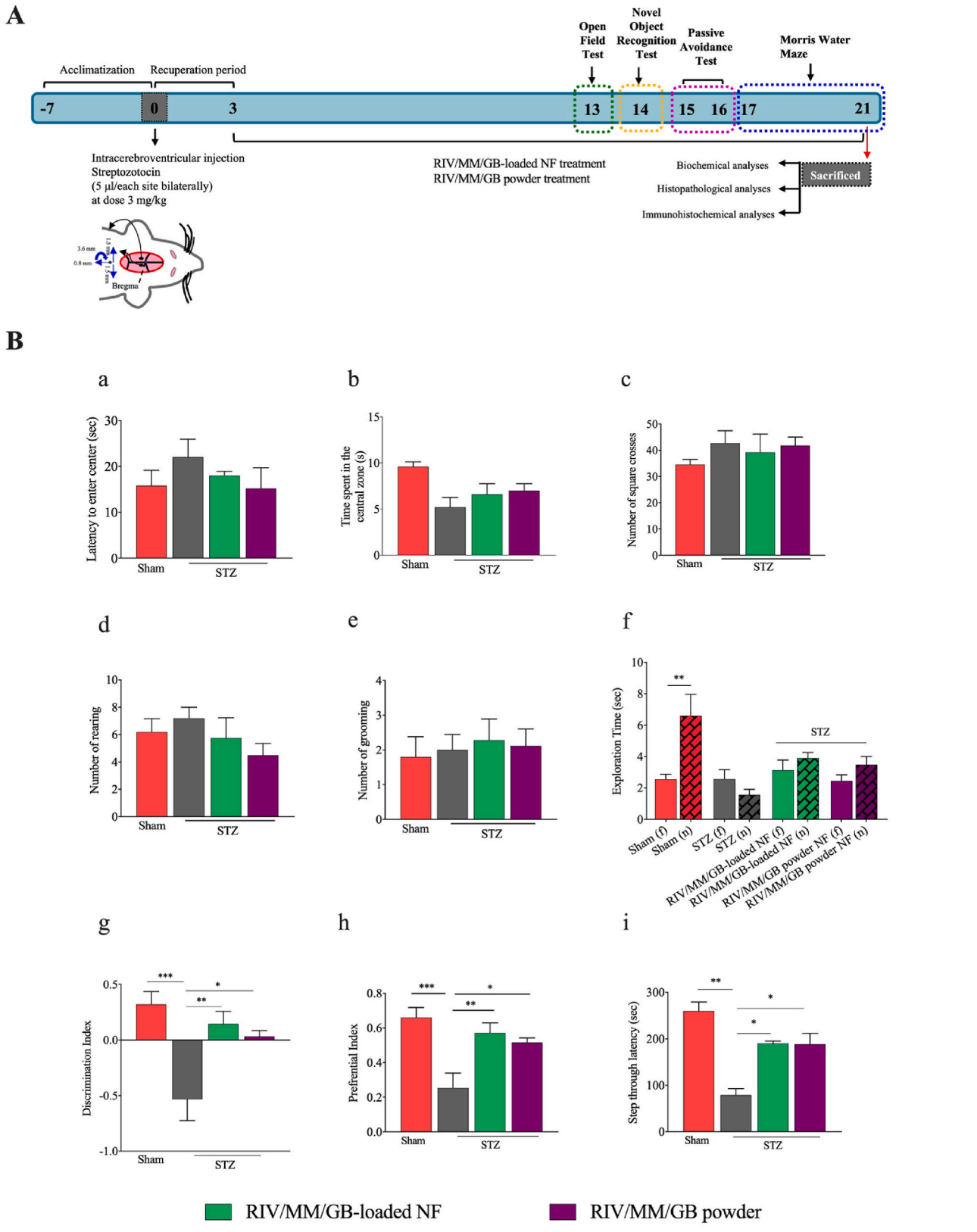

Fig. 6. A. Schematic Illustration and B. Effect of RIV/MM/GB-loaded NF treatment on OFT, NORT, and PAT; a) latency to enter the center, b) time spent in the central zone, c) the number of square crosses, d) the number of grooming, e) the number of rearing, f) exploration time, g) discrimination index, h) preferential index, and i) step-through latency. Significance differences were found at *p < 0.05, **p < 0.01 and ***p < 0.001.

considered. During 4 days of training in the MWM test, the escape latency to reach the underwater platform gradually decreased in all groups. Although there is no difference between the groups' access to the platform on the first day, there are various degrees of differences between groups on the second day. Mean escape latency was significantly ($p < 0.05$) longer in the AD group compared to the sham group, indicating a decrease in learning performance due to STZ injection. In addition, the access time of the RIV/MM/GB-loaded NF group to the platform had been remarkably ($p < 0.05$) shortened compared to the AD group. This decreased escape latency in the rats of the RIV/MM/GB-loaded NF group continued to decrease gradually during whole experimental days (Fig. 7a).

In the case of working memory, path length in all groups during the trial test was evaluated. The mean pathlength was notably ($p < 0.001$) prolonged in the AD group compared with the sham group, while the length of the road by the RIV/MM/GB-loaded NF group in the water tank decreased significantly on the 4th day (Fig. 7b). The data indicate that the absence of changes in the swimming speed of the rats included in the experiment during the entire test period. This proves that the motor functions of all groups were similar (Fig. 7c). Probe testing was performed with the platform removed on the last day of the MWM test. The percentage of time spent in the target quadrant was decreased significantly ($p < 0.01$) in the AD group compared with the sham group (Fig. 7d). Treatment with RIV/MM/GB-loaded NFs reversed cognitive deficits compared with the AD group. The RIV/MM/GB powder group displayed minor changes in tracking compared to the RIV/MM/GB-loaded NF group. On the other hand, rats in the treatment group spent more time in the target quadrant (Fig. 7e), whereas rats in the AD group were unable to recall the exact location of the platform, showing a mean distribution curve in the four quadrants of the platform.

3.13. Biochemical analysis

To further investigate the neuroprotective effects of RIV/MM/GB-loaded NF on STZ-induced rats, we determined the biochemical changes in the hippocampus after the MWM task. As shown in Fig. 7f and h, the levels of β-amyloid and Tau in AD rats were importantly increased compared to the sham group ($p < 0,01$). Both these two biomarkers levels belonging to RIV/MM/GB-loaded NF and RIV/MM/GB powder groups showed a significant decrease ($p < 0.01$ and $p < 0.05$, respectively) compared to the AD group. An important increase in APP level ($p < 0.001$) was noticed in the AD group as compared to the sham group (Fig. 7g). Treatment of RIV/MM/GB-affected NF reversed this increase compared with the AD group. Administration of RIV/MM/GB-loaded NF significantly inhibited the increase of GSK-3β in the brain of AD rats (Fig. 7i). The elevation of the AChE level in the AD group appears to be reversed by RIV/MM/GB-loaded NF (Fig. 7j). An important increase in the TNF-α level was noticed in the hippocampus of AD rats compared to that in sham rats (Fig. 7k). However, drug-loaded NF treatment reversed this increase in TNF-α levels. There was not any important difference between all groups in the BDNF level (Fig. 7l).

3.14. Histological analysis

When both the cerebral cortex and hippocampus were histologically observed by H&E staining, sham rats demonstrated regular morphology (Fig. 8). In the AD group, severe degeneration of neurons with pyknotic nuclei, perineuronal and perivascular edema, and inflammatory cell infiltration were observed in both the cerebellar cortex (Fig. 8B) and hippocampus (Fig. 8F). There was a mild degeneration of neurons in both treatment groups (Fig. 8C, D, and G, H) in comparison to the AD group. It was found that RIV/MM/GB-loaded NF application showed more neuronal regeneration than RIV/MM/GB powder in both regions.

3.15. Immunohistochemistry analysis

β-amyloid plaque accumulation was detected in the hippocampus and cortex, as indicated by the brown staining in the extracellular space of the AD group (Fig. 9 B, F). There were more positively stained plaques in the AD group compared with the sham group ($p < 0.001$) (Fig. 9A and E), whereas, less in RIV/MM/GB powder (Fig. 9C, G) and RIV/MM/GB-loaded NF groups (Fig. 9D and H) in comparison to the AD group. Statically, β-amyloid immunostaining was detected less in RIV/MM/GB-loaded NF group ($p < 0.001$) than RIV/MM/GB powder group ($p < 0.01$) in both these two areas when compared to the AD group.

For tau immunohistochemistry, in the cortical and hippocampal tissues, while tau phosphorylation was significantly increased in the AD group ($p < 0,001$) (Fig. 10B and F) in comparison to the sham group (Fig. 10A and E), there was less tau phosphorylation in RIV/MM/GB powder (Fig. 10C and G) and RIV/MM/GB-loaded NF groups (Fig. 10D and H). In the cortex, the anti-tau immuno-staining statically decreased more in the RIV/MM/GB-loaded NF ($p < 0.01$) than in the RIV/MM/GB powder group ($p < 0.05$) in comparison to the AD group. In the hippocampus, the RIV/MM/GB-loaded NF group showed statically more decreased immuno-staining ($p < 0.001$) than RIV/MM/GB powder group ($p < 0.01$) in comparison to the AD group.

4. Discussion

In the present study, it was aimed that the neuroprotective potential of RIV/MM/GB-loaded NF treatment was investigated in the icv-STZ-induced rat model of AD. Based on our data, RIV/MM/GB-loaded NF improved icv-STZ-induced cognition disorders in a pharmaceutical drug form different from conventional drug forms by decreasing β-amyloid accumulation and tau phosphorylation, increasing cholinergic transmission, lowering GSK-3β, APP, and TNF-α levels in the hippocampus. STZ injection at a sub-diabetogenic dose leads to a series of biochemical changes in the brain structure, which ultimately leads to cognitive disorders similar to sporadic Alzheimer's pathology [57]. In this study, a triple-drug combination-loaded NF treatment was produced for the sublingual drug delivery route to increase the bioavailability for AD patients and applied in the AD animal model for the first time. We chose this method of administration to benefit from the advantage of the sublingual application [20].

The FTIR spectra showed the basic characteristic peaks of RIV, MM, and GB in RIV/MM/GB-loaded NF. This data suggests that there are chemical interactions between PVA/PVP blend and drugs in NFs [44–48]. The results obtained from the DSC showed that Tg and Tm values changed after loading the drugs in the fibers due to the crystalline nature of the drug. Moreover, the fiber diameter of drug-loaded fibers with high Tg values was larger than that of pure fibers with low Tg values. Diffraction patterns of pure RIV, MM, and GB showed sharp crystalline peaks while these peaks were observed as slightly attenuated in RIV/MM/GB-loaded NF [54–56,58]. The tensile test showed that drug-loaded NFs have better mechanical strength and a more flexible structure than pure NFs [59]. NFs were suitable for the sublingual application although they had a strong structure. All characterization tests indicated that RIV/MM/GB-loaded NF is suitable for *in vivo* applications. In sublingual administration, the pharmaceutical formulation is expected to be immediately wet and disintegrate when placed under the tongue and rapidly absorbed. The produced NFs showed dramatically good wetting, disintegration, and dissolution properties. Drugs with poor solubility rates have less absorption; hence, their bioavailability decreases. GB's dissolution rate was improved by loading GB into fibers, and it was observed that the efficiency of treatment was increased by loading drugs in fibers.

The evaluation of the cytotoxicity of pure and RIV/MM/GB-loaded NFs showed that NFs did not own any cytotoxic effect, but the viability of fibroblasts on pure NF increased in comparison to RIV/MM/GB-loaded NF and control groups. On the other hand, DB-SCs showed

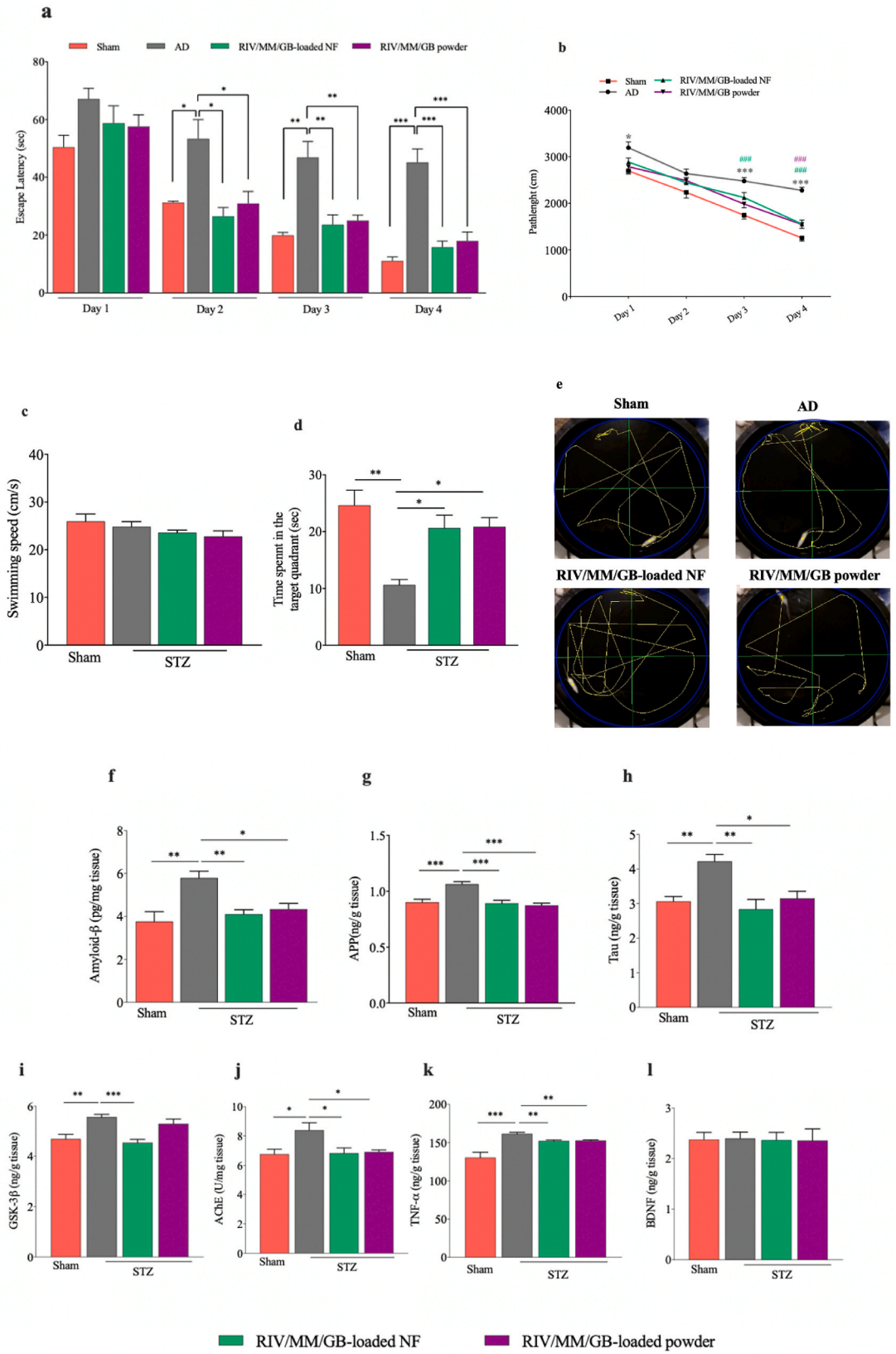

Fig. 7. Spatial learning and memory in Morris water maze (MWM) (a–e). a) mean escape latency to reach the hidden platform b) path length, c) swimming speed, d) time spent in target quadrant time, and e) the swimming path diagram. Effects of drug-loaded NF treatment on the levels of biochemical parameters (protein levels measured by ELISA) in the hippocampus (f–l): f) Amyloid-β, g) APP, h) Tau, i) GSK-3β, j) AChE, k) TNF-α and l) BDNF. Differences in significance were found at *$p <$ 0.05, **$p < 0.01$, and ***$p <$ 0,001.

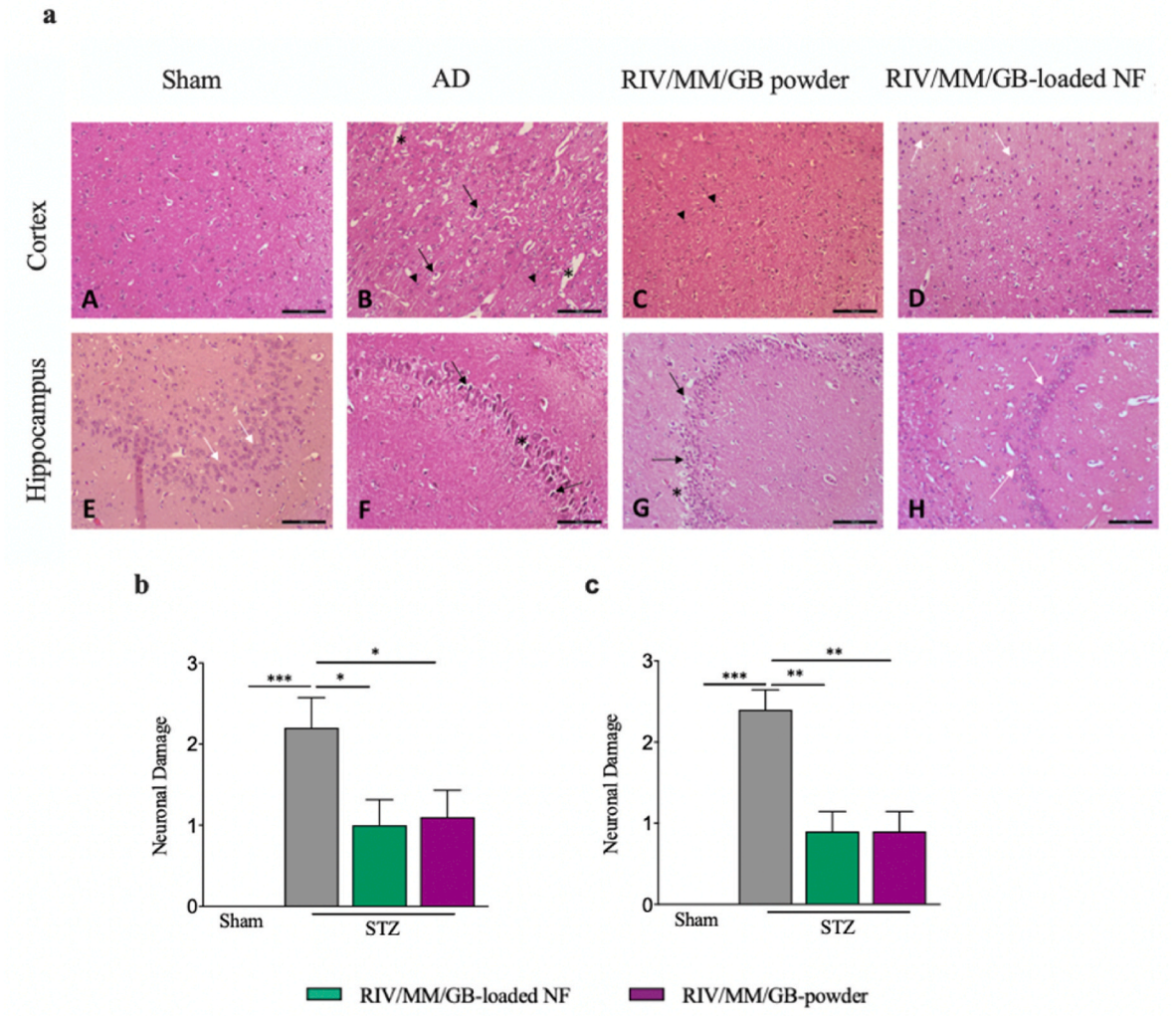

Fig. 8. a) Photomicrographs of the cerebral cortex and hippocampus (CA2) regions of brain tissues in the different experimental groups of rats. A and E: Sham groups, regular cerebral cortex and hippocampus, respectively; B and F: AD groups, degenerated neurons (arrow), pericellular/perivascular edema (*), and inflammatory cell infiltration (filled triangle); C and G: RIV/MM/GB powder group, mild perivascular edema (*) and inflammatory cell infiltration in the cerebral cortex and hippocampus, respectively; D and H: Normal neurons and pyramidal cells (white arrow) in both brain regions. Neuronal damage scoring in b) hippocampal area c) cortical area of the animal groups. H&E staining, original magnifications: 100 μm.

resistance to the released level of RIV/MM/GB from NFs and surviving cells could be observed after 7 days. The increasingly accumulated level of drug in the limited volume of culture medium caused a slight loss of cell viability but it was not significant. Further, such adverse effect was not observed *in vivo*. Although the cell numbers were reduced *in vitro*, the effect of pure and RIV/MM/GB-loaded NFs improved the neuronal differentiation of DP-SCs and retained a notable potential for neuronal differentiation [60]. The expression of BDNF significantly improved after culture on RIV/MM/GB-loaded NFs and chemical induction further increased its expression. The elevated level of neurotrophic factor, BDNF, was illustrated to improve cognitive deficits in AD animal models and patients [61]. The reduction in cognitive impairment can be explained by an increase in intracellular BDNF. The enhancement of neuronal and glial differentiation (TUBB3 and GFAP, respectively), as well as the survival of existing cells in the culture, could be maintained by the secretion of trophic factors, BDNF. The improving number of cells might be explained by the supporting effect of BDNF during the culture and the differentiation. Supporting the BDNF biosynthesis by RIV/MM/GB-loaded NFs could lead to an increased level of BDNF, which might interfere with the ongoing degeneration and prevent cognitive decline [61]. Neuronal differentiation was also mediated by the Neurog2 expression, and the increased activity and expression of Neurog2 could be related to the accumulation of β-amyloid precursor protein [62]. Due to the effect of drugs-loaded NFs, the expression of Neurog2, which is an Alzheimer's β-amyloid responsive gene, improved significantly. The expression of the pro-neuronal genes, NeuroD1, and nestin, also supports cognitive restoration under the effect of curcumin-encapsulated PLGA nanoparticles [63]. Similarly, RIV/MM/GB-loaded NF might improve the expression of cell proliferation (nestin) and neuronal differentiation (neuroD1) genes, leading to the inhibition of the β-amyloid aggregation [64]. The stem cells on pure NFs were differentiated, but with lower efficiency compared to RIV/MM/GB-loaded NFs. The fibrous surface was not sufficient to initiate total cell differentiation into neuronal cells, but it can provide a loose cell attachment. These topographical surfaces which replicate the natural structure of neuron cell niche to some degree through micro- or nanoscale geometry might gain the functionality of the stem cells to support the neurogenic differentiation [65].

The fact that the OFT results did not differ significantly between groups in terms of locomotion ability is compatible with other studies that prefer this model in the AD disease [66]. An enhancement in discrimination and preferential indices in the NORT that was applied to

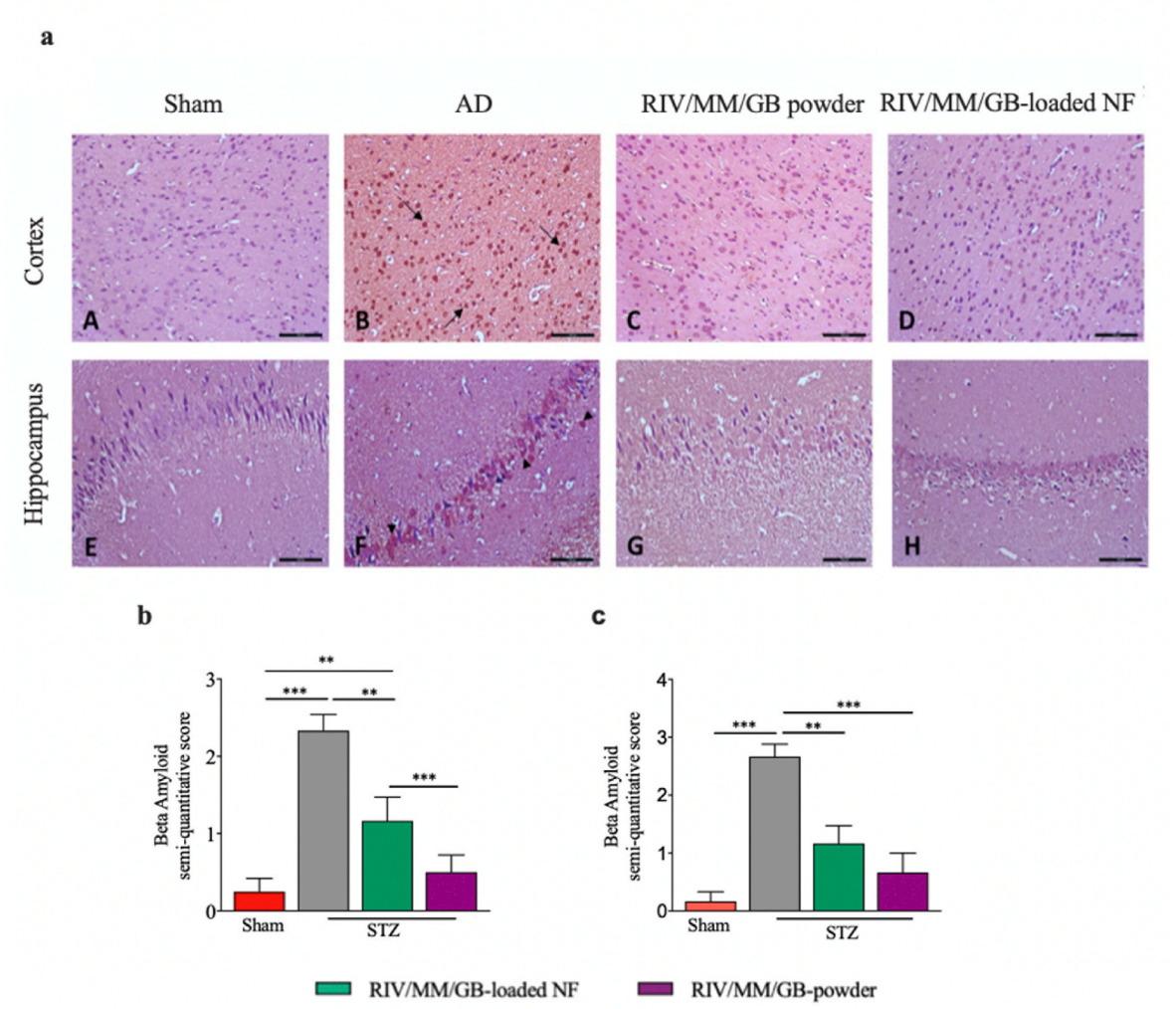

Fig. 9. Anti-β-amyloid ((anti-β-amyloid (ABCAM, ab10148)) immunohistochemistry in the cerebral cortex and hippocampus (CA2) regions of experimental rat groups (Scale bar: 100 μm, n = 3). a) The AD group showed severe amyloid plaques formation (arrows) in the cortex (B), and severe immunoreactivity (filled triangles) in the neuronal body of the hippocampal area (F) when compared with the sham group (Fig. A and E, respectively). RIV/MM/GB-loaded NF and RIV/MM/GB powder groups significantly attenuated this pathology (C, G, and D, H, respectively). →: Positive staining. β-amyloid semi-quantitative scoring in b) hippocampal area, c) cortical area of the animal groups. Significance differences were found at $^{**}p < 0.01$ and $^{***}p < 0.001$.

evaluate short-term memory ability pointed out that RIV/MM/GB-loaded NF treatment prevented icv-STZ-induced memory impairments [66]. The PAT aims to measure a conditional stimulating of learning ability to assess emotional memory (short-time memory) in case of fear/anxiety [67]. In line with previous studies, according to the step-through latency values, memory acquisition was damaged in animals receiving STZ. Animals treated with RIV/MM/GB-loaded NF avoided crossing the dark area with a conditioned response 24 h after the electric shock was subjected. Our findings confirmed that icv-STZ-administered rats have a longer escape latency for four days than other groups, indicating that STZ had a detrimental effect on learning and memory. From the second day, the similarity between the RIV/MM/GB-loaded NF and RIV/MM/GB powder groups of shortening time to reach the hidden platform shows the favourable effects of our treatments on cognitive functions. From another point of view, the length of the path that the STZ-induced animals take in the pool for 4 days is quite long compared to other groups. In the probe test, STZ-induced rats spent more time reaching the target quadrant, without any difference in the swimming speed of all groups. Our findings suggest that this deficiency in icv-STZ memory retrieval was reverted by RIV/MM/GB-loaded NF. Furthermore, a decrease in the entrance of AD animals to the former located platform site was observed, while the animals in the treatment and sham groups entered the target quadrant more. Our results suggested that RIV/MM/GB-loaded NF could ameliorate learning and spatial memory function.

β-amyloid accumulation, decrease in cholinergic transmission and BDNF increase in GSK-3β, and an increase of inflammatory cytokines such as TNF-α, which are in the pathogenesis of Alzheimer's, are determined as targets in the treatment strategy. RIV is known to regulate cholinergic transmission by inhibiting cholinesterase enzyme and reducing β-amyloid deposition. On the other hand, MM is a drug that prevents β-amyloid accumulation and inhibits tau phosphorylation. Besides, GB can reduce inflammatory cytokines such as TNF-α and regulate GSK-β activation and β-amyloid deposition. Administration of STZ by the icv leads to many biochemical changes in the brain that mimic AD pathophysiology. Icv-STZ is accepted as an AD animal model in the experimental studies due to its effects in the form of increasing β-amyloid level, tau hyperphosphorylation, GSK-3β activity, APP level, and decreasing BDNF in the brain. In our study, icv administration of STZ showed a significant increase in β-amyloid, tau, AChE, GSK-3β, APP, and TNF-α levels. However, RIV/MM/GB-loaded NF treatment was able to convert these parameters to be close to the sham group. RIV/MM/GB-loaded NF remarkably reduced the levels of β-amyloid, tau, APP, AChE, and TNF-α when compared with the AD group. On the other hand,

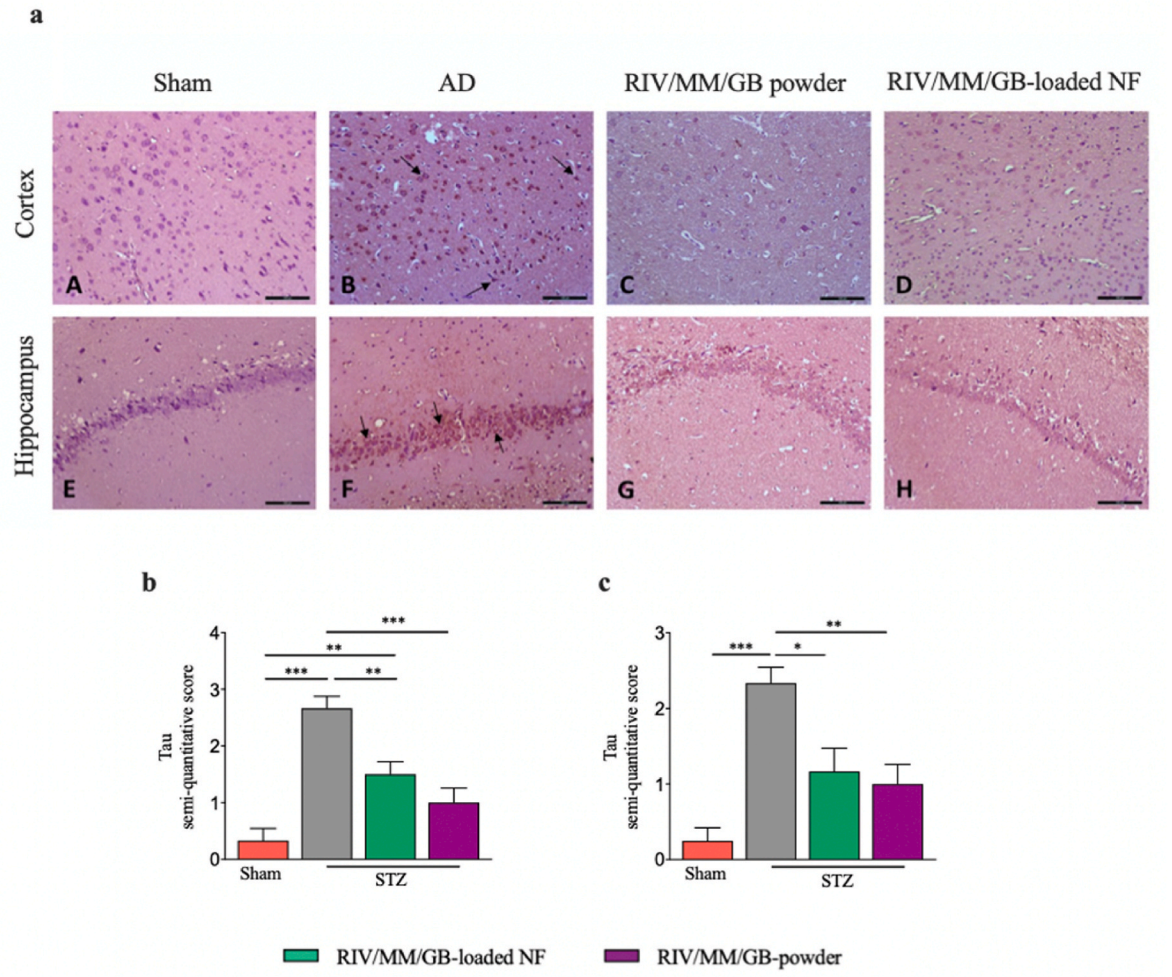

Fig. 10. Anti-tau (anti-tau; ABCAM, ab131354) immunohistochemistry in the cortex and hippocampus (CA2) regions of the experimental rat groups (Scale bar: 100 μm). a) The AD group showed severe immunoreactivity (arrows) in the neuronal body in the cortex and hippocampal region (B and F) when compared with the sham group (A and E). It was observed that this immunoreactivity was dramatically reduced with the administration of RIV/MM/GB powder and drug-loaded NF (C, G, and D, H, respectively). →: Positive staining. Anti-tau Semi-quantitative scoring in b) hippocampal area, c) cortical area of animal group. A significant difference was observed at $^{**}p < 0.01$ and $^{***}p < 0.001$.

significant cortical and hippocampal neuronal damage in the AD group improved with RIV/MM/GB-loaded NFs. These all data suggest the hopeful ameliorative potential of RIV/MM/GB-loaded NF in managing AD through multiple targets.

5. Conclusion

RIV/MM/GB-loaded NF was successfully produced by ES and the results of the evaluations showed that it is suitable for the sublingual route according to the characterization, disintegration, and dissolution tests. These fibers showed no toxic effects and stem cells exhibited improved neuronal differentiation properties under the effect of RIV/MM/GB-loaded NFs. DP-SCs on drug-loaded NF improved survival rate after 7 days while demonstrating increased expression of neuronal markers such as TUBB3, BDNF, and Nestin. The RIV/MM/GB-loaded NF treatment also improved short-term memory impairment and improved memory, learning ability, and spatial exploration ability better than RIV/MM/GB powder according to behaviour tests in icv-STZ-induced AD animal model. Consistent with these observations RIV/MM/GB-loaded NF ameliorated AD pathologies by reducing β-amyloid deposition, tau phosphorylation, and cholinergic transmission in which alteration of GSK-3β, APP, AChE, and TNF-α might be involved. It was revealed that the increased degeneration of neurons in the cortex and hippocampus regions with icv-STZ induction was significantly reduced with the RIV/MM/GB-loaded NF application because it reversed tissue damages resulting from β-amyloid plaque accumulation and tau phosphorylation. Finally, our findings take a promising step in developing a new therapeutic strategy with the advantages such as increased bioavailability, decreased frequency of dosage and systemic side effects, and increased patient compliance for the treatment of AD by targeting multifunctional alterations.

CRediT authorship contribution statement

Servan Veysanoglu: Conceptualization, Investigation, Methodology; Busra Ertas: Conceptualization, Investigation, Data curation, Writing - original draft, Project administration; Ece Guler: Methodology, Validation; Fadime Topal: Investigation, Writing - original draft, Software; Gul Sinemcan Ozcan: Methodology, Resources; Gokhan Duruksu: Methodology; Burak Ece: Software, Validation; Cansun Sahin Cam: Visualization; Oguzhan Aydemir: Methodology; Muhammet Emin Cam: Conceptualization, Supervision, Validation, Writing - review & editing.

Declaration of competing interest

Authors all declare that there is no existing conflict of interest.

Data availability

Data will be made available on request.

Acknowledgments

Servan Veysanoglu and Busra Ertas contributed equally to this work. This project was supported by a TUBITAK 2209-A Research Projects Program Grant (Scientific and Technological Research Council of Turkey-TUBITAK, Project Number: 1919B011903626).

Appendix A. Supplementary data

Supplementary data to this article can be found online at https://doi.org/10.1016/j.jddst.2023.104691.

References

[1] T.O. Tobore, On the etiopathogenesis and pathophysiology of Alzheimer's disease: a comprehensive theoretical review, J Alzheimers Dis 68 (2) (2019) 417–437.
[2] T.Y. Fung, A. Iyaswamy, S.G. Sreenivasmurthy, S. Krishnamoorthi, X.J. Guan, Z. Zhu, C.F. Su, J. Liu, Y. Kan, Y. Zhang, H.L.X. Wong, M. Li, Klotho an autophagy stimulator as a potential therapeutic target for Alzheimer's disease: a review, Biomedicines 10 (3) (2022).
[3] S.G. Sreenivasmurthy, A. Iyaswamy, S. Krishnamoorthi, R.N. Reddi, A.K. Kammala, K. Vasudevan, S. Senapati, Z. Zhu, C.F. Su, J. Liu, X.J. Guan, K.K. Chua, K. H. Cheung, H. Chen, H.J. Zhang, Y. Zhang, J.X. Song, S.S. Kumar Durairajan, M. Li, Bromo-protopine, a novel protopine derivative, alleviates tau pathology by activating chaperone-mediated autophagy for Alzheimer's disease therapy, Front. Mol. Biosci. 9 (2022), 1030534.
[4] K. Selvarasu, A.K. Singh, A. Iyaswamy, S. Gopalkrishnashetty Sreenivasmurthy, S. Krishnamoorthi, A.K. Bera, J.D. Huang, S.S.K. Durairajan, Reduction of kinesin I heavy chain decreases tau hyperphosphorylation, aggregation, and memory impairment in Alzheimer's disease and tauopathy models, Front. Mol. Biosci. 9 (2022), 1050768.
[5] P.T. Francis, M.J. Ramírez, M.K. Lai, Neurochemical basis for symptomatic treatment of Alzheimer's disease, Neuropharmacology 59 (4) (2010) 221–229.
[6] D. Olivares, V.K. Deshpande, Y. Shi, D.K. Lahiri, N.H. Greig, J.T. Rogers, X. Huang, N-methyl D-aspartate (NMDA) receptor antagonists and memantine treatment for Alzheimer's disease, vascular dementia and Parkinson's disease, Curr. Alzheimer Res. 9 (6) (2012) 746–758.
[7] J. Fang, L. Wang, T. Wu, C. Yang, L. Gao, H. Cai, J. Liu, S. Fang, Y. Chen, W. Tan, Q. Wang, Network pharmacology-based study on the mechanism of action for herbal medicines in Alzheimer treatment, J. Ethnopharmacol. 196 (2017) 281–292.
[8] B. Vellas, N. Coley, P.J. Ousset, G. Berrut, J.F. Dartigues, B. Dubois, H. Grandjean, F. Pasquier, F. Piette, P. Robert, J. Touchon, P. Garnier, H. Mathiex-Fortunet, S. Andrieu, Long-term use of standardised Ginkgo biloba extract for the prevention of Alzheimer's disease (GuidAge): a randomised placebo-controlled trial, Lancet Neurol. 11 (10) (2012) 851–859.
[9] B.J. Diamond, S.C. Shiflett, N. Feiwel, R.J. Matheis, O. Noskin, J.A. Richards, N. E. Schoenberger, Ginkgo biloba extract: mechanisms and clinical indications, Arch. Phys. Med. Rehabil. 81 (5) (2000) 668–678.
[10] L.-D. Zhang, L. Ma, L. Zhang, J.-G. Dai, L.-G. Chang, P.-L. Huang, X.-Q. Tian, Hyperbaric oxygen and ginkgo biloba extract ameliorate cognitive and memory impairment via nuclear factor kappa-B pathway in rat model of Alzheimer's disease, Chin. Med. J. 128 (22) (2015) 3088–3093.
[11] C. Reitz, R. Mayeux, Alzheimer disease: epidemiology, diagnostic criteria, risk factors and biomarkers, Biochem. Pharmacol. 88 (4) (2014) 640–651.
[12] J.L. Cummings, G. Tong, C. Ballard, Treatment combinations for Alzheimer's disease: current and future pharmacotherapy options, J Alzheimers Dis 67 (3) (2019) 779–794.
[13] W.J. Fessel, Concordance of several subcellular interactions initiates Alzheimer's dementia: their reversal requires combination treatment, Am J Alzheimers Dis. Other Demen. 32 (3) (2017) 166–181.
[14] S. Tomaszewski, S. Gauthier, A. Wimo, P. Rosa-Neto, Combination therapy of anti-tau and anti-amyloid drugs for disease modification in early-stage Alzheimer's disease: socio-economic considerations modeled on treatments for tuberculosis, HIV/AIDS and breast cancer, J Prev. Alzheimers Dis. 3 (3) (2016) 164–172.
[15] B. Schmitt, T. Bernhardt, H.J. Moeller, I. Heuser, L. Frolich, Combination therapy in Alzheimer's disease: a review of current evidence, CNS Drugs 18 (13) (2004) 827–844.
[16] M. Correia Sde, L.S. Morillo, W. Jacob Filho, L.L. Mansur, Swallowing in moderate and severe phases of Alzheimer's disease, Arq. Neuropsiquiatr 68 (6) (2010) 855–861.
[17] J. Jin, G.E. Sklar, V. Min Sen Oh, S. Chuen Li, Factors affecting therapeutic compliance: a review from the patient's perspective, Therapeut. Clin. Risk Manag. 4 (1) (2008) 269–286.
[18] Y. Jiang, C. Liu, W. Zhai, N. Zhuang, T. Han, Z. Ding, The optimization design of lactoferrin loaded HupA nanoemulsion for targeted drug transport via intranasal route, Int. J. Nanomed. 14 (2019) 9217–9234.
[19] T. Hayashi, M. To, J. Saruta, C. Sato, Y. Yamamoto, Y. Kondo, T. Shimizu, Y. Kamata, K. Tsukinoki, Salivary lactoferrin is transferred into the brain via the sublingual route, Biosci. Biotechnol. Biochem. 81 (7) (2017) 1300–1304.
[20] S. Hua, Advances in nanoparticulate drug delivery approaches for sublingual and buccal administration, Front. Pharmacol. 10 (2019) 1328, 1328.
[21] M.E. Cam, B. Ertas, H. Alenezi, A.N. Hazar-Yavuz, S. Cesur, G.S. Ozcan, C. Ekentok, E. Guler, C. Katsakouli, Z. Demirbas, D. Akakin, M.S. Eroglu, L. Kabasakal, O. Gunduz, M. Edirisinghe, Accelerated diabetic wound healing by topical application of combination oral antidiabetic agents-loaded nanofibrous scaffolds: an in vitro and in vivo evaluation study, Mater. Sci. Eng. C 119 (2021), 111586.
[22] S. Thakkar, M. Misra, Electrospun polymeric nanofibers: new horizons in drug delivery, Eur. J. Pharmaceut. Sci. 107 (2017) 148–167.
[23] P. Sati, P. Dhyani, I.D. Bhatt, A. Pandey, Ginkgo biloba flavonoid glycosides in antimicrobial perspective with reference to extraction method, J. Tradit. Complement. Med. 9 (1) (2019) 15–23.
[24] M.F. Ismail, A.N. Elmeshad, N.A. Salem, Potential therapeutic effect of nanobased formulation of rivastigmine on rat model of Alzheimer's disease, Int. J. Nanomed. 8 (2013) 393–406.
[25] M. Stazi, O. Wirths, Chronic memantine treatment ameliorates behavioral deficits, neuron loss, and impaired neurogenesis in a model of Alzheimer's disease, Mol. Neurobiol. 58 (1) (2021) 204–216.
[26] P.A. Kwak, S.C. Lim, S.R. Han, Y.M. Shon, Y.I. Kim, Supra-additive neuroprotection by renexin, a mixed compound of ginkgo biloba extract and cilostazol, against apoptotic white matter changes in rat after chronic cerebral hypoperfusion, J. Clin. Neurol. 8 (4) (2012) 284–292.
[27] M.E. Cam, S. Cesur, T. Taskin, G. Erdemir, D.S. Kuruca, Y.M. Sahin, L. Kabasakal, O. Gunduz, Fabrication, characterization and fibroblast proliferative activity of electrospun Achillea lycaonica-loaded nanofibrous mats, Eur. Polym. J. 120 (2019), 109239.
[28] M.E. Cam, A.N. Hazar-Yavuz, S. Cesur, O. Ozkan, H. Alenezi, H. Turkoglu Sasmazel, M. Sayip Eroglu, F. Brako, J. Ahmed, L. Kabasakal, G. Ren, O. Gunduz, M. Edirisinghe, A novel treatment strategy for preterm birth: intra-vaginal progesterone-loaded fibrous patches, Int. J. Pharm. 588 (2020), 119782.
[29] M.E. Cam, M. Crabbe-Mann, H. Alenezi, A.N. Hazar-Yavuz, B. Ertas, C. Ekentok, G. S. Ozcan, F. Topal, E. Guler, Y. Yazir, M. Parhizkar, M. Edirisinghe, The comparision of glybenclamide and metformin-loaded bacterial cellulose/gelatin nanofibres produced by a portable electrohydrodynamic gun for diabetic wound healing, Eur. Polym. J. 134 (2020), 109844.
[30] F. Topal, B. Ertas, E. Guler, F. Gurbuz, G.S. Ozcan, O. Aydemir, V.G. Bocekci, G. Duruksu, C. Sahin Cam, Y. Yazir, O. Gunduz, M.E. Cam, A novel multi-target strategy for Alzheimer's disease treatment via sublingual route: donepezil/memantine/curcumin-loaded nanofibers, Biomater, Advisor 138 (2022), 212870.
[31] U.E. Illangakoon, H. Gill, G.C. Shearman, M. Parhizkar, S. Mahalingam, N. P. Chatterton, G.R. Williams, Fast dissolving paracetamol/caffeine nanofibers prepared by electrospinning, Int. J Pharm. 477 (1–2) (2014) 369–379.
[32] R. Kapil, S. Dhawan, B. Singh, Development and validation of a spectrofluorimetric method for the estimation of rivastigmine in formulations, Indian J. Pharmaceut. Sci. 71 (2009) 585–589.
[33] H.-J. Maeng, S.-U. Choi, D.-J. Jang, D.W. Lee, B.-N. Ahn, M.-K. Choi, I.-S. Song, K. H. Cho, Validation and application of a simple reverse phase HPLC method for in vitro dissolution studies of memantine hydrochloride tablet, J. Pharm. Investig. 45 (5) (2015) 415–421.
[34] W. Wang, Q. Kang, N. Liu, Q. Zhang, Y. Zhang, H. Li, B. Zhao, Y. Chen, Y. Lan, Q. Ma, Q. Wu, Enhanced dissolution rate and oral bioavailability of Ginkgo biloba extract by preparing solid dispersion via hot-melt extrusion, Fitoterapia 102 (2015) 189–197.
[35] G. Duruksu, S. Polat, L. Kayiş, N. Ekimci Gürcan, G. Gacar, Y. Yazir, Improvement of the insulin secretion from beta cells encapsulated in alginate/poly-L- histidine/alginate microbeads by platelet-rich plasma, Turk. J. Biol. 42 (4) (2018) 297–306.
[36] E. Karaöz, P.C. Demircan, O. Sağlam, A. Aksoy, F. Kaymaz, G. Duruksu, Human dental pulp stem cells demonstrate better neural and epithelial stem cell properties than bone marrow-derived mesenchymal stem cells, Histochem. Cell Biol. 136 (4) (2011) 455–473.
[37] S.S. Gocmez, T.D. Şahin, Y. Yazir, G. Duruksu, F.C. Eraldemir, S. Polat, T. Utkan, Resveratrol prevents cognitive deficits by attenuating oxidative damage and inflammation in rat model of streptozotocin diabetes induced vascular dementia, Physiol. Behav. 201 (2019) 198–207.
[38] M. Salkovic-Petrisic, A. Knezovic, S. Hoyer, P. Riederer, What have we learned from the streptozotocin-induced animal model of sporadic Alzheimer's disease, about the therapeutic strategies in Alzheimer's research, J. Neural. Transm. 120 (1) (2013) 233–252.
[39] P.K. Kamat, A. Kalani, S. Rai, S.K. Tota, A. Kumar, A.S. Ahmad, Streptozotocin intracerebroventricular-induced neurotoxicity and brain insulin resistance: a therapeutic intervention for treatment of sporadic Alzheimer's disease (sAD)-Like pathology, Mol. Neurobiol. 53 (7) (2016) 4548–4562.
[40] P. Grieb, Intracerebroventricular streptozotocin injections as a model of Alzheimer's disease: in search of a relevant mechanism, Mol. Neurobiol. 53 (3) (2016) 1741–1752.
[41] H. Abbas, N.S.E. Sayed, N. Youssef, M.E.G. P, M.R. Mousa, A.M. Fayez, M. A. Elsheikh, Novel luteolin-loaded chitosan decorated nanoparticles for brain-targeting delivery in a sporadic Alzheimer's disease mouse model: focus on antioxidant, anti-inflammatory, and amyloidogenic pathways, Pharmaceutics 14 (5) (2022).
[42] A.P. Muller, G.K. Ferreira, A.J. Pires, G. de Bem Silveira, D.L. de Souza, J. A. Brandolfi, C.T. de Souza, M.M.S. Paula, P.C.L. Silveira, Gold nanoparticles prevent cognitive deficits, oxidative stress and inflammation in a rat model of

sporadic dementia of Alzheimer's type, Mater Sci. Eng. C Mater. Biol. Appl. 77 (2017) 476–483.
[43] B. Ertas, F. Topal, R. Gulhan, R. Yanardag, O. Sacan, G. Sener, J Res. in Pharm. 25 (5) (2021) 589–599.
[44] M. Chuong, C. Kelley, Y. Muhammad, T. Caputo, J. Gomes, D. Oliveira, A. Peixoto, B. Pereira, W. Rizg, C. Vazquez, T. Zacaron, S. Nguyen, D. Williams, Investigating effect of water of hydration on active pharmaceutical ingredients in a water-sensitive dosage form, J Anal Sci Technol 9 (2018) 7.
[45] P. Prapatpong, T. Techa-In, W. Padungpuak, S. Buranaphalin, L. Suntornsuk, HPLC-fluorescent analysis of memantine: an investigation on fluorescent derivative formation, J. Chem. 2015 (2015) 1–7.
[46] M.E. Collinson, B. Mösle, P. Finch, A. Scott, R. Wilson, The preservation of plant cuticle in the fossil record: a chemical and microscopical investigation, Anc. Biomol. 2 (1998) 251–265.
[47] I. Korbag, S. Saleh, Studies on the formation of intermolecular interactions and structural characterization of polyvinyl alcohol/lignin film, Int. J. Environ. Stud. (2016) 1–10.
[48] R. Bryaskova, D. Pencheva, S. Nikolov, T. Kantardjiev, Synthesis and comparative study on the antimicrobial activity of hybrid materials based on silver nanoparticles (AgNPs) stabilized by polyvinylpyrrolidone (PVP), J. Chem. Biol. 4 (2011) 185–191.
[49] M. Magalhães, R. Toledo Filho, E. Fairbairn, Durability under thermal loads of polyvinyl alcohol fibers, Materia 18 (2013) 1587–1595.
[50] Y. Ge, An investigation into the mechanisms of rapid release of standard extract from Ginkgo biloba leaf in polyethylene glycol 6000 solid dispersions, Yakugaku Zasshi 130 (3) (2010) 425–430.
[51] M. Fazil, S. Md, S. Haque, M. Kumar, S. Baboota, J.K. Sahni, J. Ali, Development and evaluation of rivastigmine loaded chitosan nanoparticles for brain targeting, Eur. J. Pharmaceut. Sci. 47 (1) (2012) 6–15.
[52] N. Mittapelly, R. Rachumallu, G. Pandey, S. Sharma, A. Arya, R.S. Bhatta, P. R. Mishra, Investigation of salt formation between memantine and pamoic acid: its exploitation in nanocrystalline form as long acting injection, Eur. J. Pharm. Biopharm. 101 (2016) 62–71.
[53] K. Pagar, P. Vavia, Rivastigmine-loaded L-lactide-depsipeptide polymeric nanoparticles: decisive formulation variable optimization, Sci. Pharm. 81 (3) (2013) 865–885.
[54] R. A, T. Devasena, Facile Synthesis of curcumin nanocrystals and validation of its antioxidant activity against circulatory toxicity in wistar rats, JNN 15 (2015) 4119–4125.
[55] V. Naranappa, S. Subramanian, N. Hellar, S. Chinnappanadar, Proton Conducting Polymer Electrolyte Based on Poly (N-Vinyl Pyrrolidone) Doped with Ammonium Iodide, 2015.
[56] G.-M. Kim, Fabrication of Bio-Nanocomposite Nanofibers Mimicking the Mineralized Hard Tissues via Electrospinning Process, 2010.
[57] T. Guardia de Souza e Silva, M.E.F. do Val de Paulo, J.R.M. da Silva, A. da Silva Alves, L.R.G. Britto, G.F. Xavier, M.R. Lopes Sandoval, Oral treatment with royal jelly improves memory and presents neuroprotective effects on icv-STZ rat model of sporadic Alzheimer's disease, Heliyon 6 (2) (2020), e03281.
[58] N. Mittapelly, R. Rachumallu, G. Pandey, S. Sharma, A. Arya, R.S. Bhatta, P. R. Mishra, Investigation of salt formation between memantine and pamoic acid: its exploitation in nanocrystalline form as long acting injection, Eur. J. Pharm. Biopharm. 101 (2016) 62–71.
[59] M.E. Cam, S. Yildiz, H. Alenezi, S. Cesur, G.S. Ozcan, G. Erdemir, U. Edirisinghe, D. Akakin, D.S. Kuruca, L. Kabasakal, O. Gunduz, M. Edirisinghe, Evaluation of burst release and sustained release of pioglitazone-loaded fibrous mats on diabetic wound healing: an in vitro and in vivo comparison study, J. R. Soc., Interface 17 (162) (2020), 20190712.
[60] J. Xiao, R. Yang, S. Biswas, Y. Zhu, X. Qin, M. Zhang, L. Zhai, Y. Luo, X. He, C. Mao, W. Deng, Neural stem cell-based regenerative approaches for the treatment of multiple sclerosis, Mol. Neurobiol. 55 (4) (2018) 3152–3171.
[61] F. Fumagalli, G. Racagni, M.A. Riva, The expanding role of BDNF: a therapeutic target for Alzheimer's disease? Pharmacogenomics 6 (1) (2006) 8–15.
[62] M. Bolós, Y. Hu, K.M. Young, L. Foa, D.H. Small, Neurogenin 2 mediates amyloid-β precursor protein-stimulated neurogenesis, J. Biol. Chem. 289 (45) (2014) 31253–31261.
[63] S.K. Tiwari, S. Agarwal, B. Seth, A. Yadav, S. Nair, P. Bhatnagar, M. Karmakar, M. Kumari, L.K. Chauhan, D.K. Patel, V. Srivastava, D. Singh, S.K. Gupta, A. Tripathi, R.K. Chaturvedi, K.C. Gupta, Curcumin-loaded nanoparticles potently induce adult neurogenesis and reverse cognitive deficits in Alzheimer's disease model via canonical Wnt/β-catenin pathway, ACS Nano 8 (1) (2014) 76–103.
[64] P.H. Reddy, M. Manczak, X. Yin, M.C. Grady, A. Mitchell, S. Tonk, C.S. Kuruva, J. S. Bhatti, R. Kandimalla, M. Vijayan, S. Kumar, R. Wang, J.A. Pradeepkiran, G. Ogunmokun, K. Thamarai, K. Quesada, A. Boles, A.P. Reddy, Protective effects of Indian spice curcumin against amyloid-β in Alzheimer's disease, J Alzheimers Dis 61 (3) (2018) 843–866.
[65] F. Guilak, D.M. Cohen, B.T. Estes, J.M. Gimble, W. Liedtke, C.S. Chen, Control of stem cell fate by physical interactions with the extracellular matrix, Cell Stem Cell 5 (1) (2009) 17–26.
[66] B. Kadıoğlu Yaman, Ö. Çevik, K. Yalman, B. Ertaş, A. Şen, G. Şener, Myrtus communis subsp. communis improved cognitive functions in ovariectomized diabetic rats, Gene 744 (2020), 144616.
[67] L. Canto-de-Souza, R. Mattioli, The consolidation of inhibitory avoidance memory in mice depends on the intensity of the aversive stimulus: the involvement of the amygdala, dorsal hippocampus and medial prefrontal cortex, Neurobiol. Learn. Mem. 130 (2016) 44–51.